



Integrin-Driven Axon Regeneration in the Spinal Cord Activates a Distinctive CNS Regeneration Program

Menghon Cheah,^{1*} Yuyan Cheng,^{2*} Veselina Petrova,³ Anda Cimpean,⁴ Pavla Jendelova,⁴  Vivek Swarup,^{2,5}  Clifford J. Woolf,³ Daniel H. Geschwind,² and  James W. Fawcett^{1,4}

¹John van Geest Centre for Brain Repair, Department of Clinical Neurosciences, University of Cambridge, Cambridge CB2 0PY, United Kingdom, ²Program in Neurogenetics, Department of Neurology, and Department of Human Genetics, David Geffen School of Medicine, University of California, Los Angeles, California 90095, ³Department of Neurobiology, Harvard Medical School; F.M. Kirby Neurobiology Center, Boston Children's Hospital, Boston, Massachusetts 02115, ⁴Centre for Reconstructive Neuroscience, Institute of Experimental Medicine Czech Academy of Science, Prague, Czech Republic, and ⁵Department of Neurobiology and Behavior, University of California, Irvine, California 92697

The peripheral branch of sensory dorsal root ganglion (DRG) neurons regenerates readily after injury unlike their central branch in the spinal cord. However, extensive regeneration and reconnection of sensory axons in the spinal cord can be driven by the expression of $\alpha 9$ integrin and its activator kindlin-1 ($\alpha 9k1$), which enable axons to interact with tenascin-C. To elucidate the mechanisms and downstream pathways affected by activated integrin expression and central regeneration, we conducted transcriptomic analyses of adult male rat DRG sensory neurons transduced with $\alpha 9k1$, and controls, with and without axotomy of the central branch. Expression of $\alpha 9k1$ without the central axotomy led to upregulation of a known PNS regeneration program, including many genes associated with peripheral nerve regeneration. Coupling $\alpha 9k1$ treatment with dorsal root axotomy led to extensive central axonal regeneration. In addition to the program upregulated by $\alpha 9k1$ expression, regeneration in the spinal cord led to expression of a distinctive CNS regeneration program, including genes associated with ubiquitination, autophagy, endoplasmic reticulum (ER), trafficking, and signaling. Pharmacological inhibition of these processes blocked the regeneration of axons from DRGs and human iPSC-derived sensory neurons, validating their causal contributions to sensory regeneration. This CNS regeneration-associated program showed little correlation with either embryonic development or PNS regeneration programs. Potential transcriptional drivers of this CNS program coupled to regeneration include *Mef2a*, *Runx3*, *E2f4*, and *Yy1*. Signaling from integrins primes sensory neurons for regeneration, but their axon growth in the CNS is associated with an additional distinctive program that differs from that involved in PNS regeneration.

Key words: autophagy; axon regeneration; integrin; sensory; signaling; spinal cord

Significance Statement

Restoration of neurologic function after spinal cord injury has yet to be achieved in human patients. To accomplish this, severed nerve fibers must be made to regenerate. Reconstruction of nerve pathways has not been possible, but recently, a method for stimulating long-distance axon regeneration of sensory fibers in rodents has been developed. This research uses profiling of messenger RNAs in the regenerating sensory neurons to discover which mechanisms are activated. This study shows that the regenerating neurons initiate a novel CNS regeneration program which includes molecular transport, autophagy, ubiquitination, and modulation of the endoplasmic reticulum (ER). The study identifies mechanisms that neurons need to activate to regenerate their nerve fibers.

Received Nov. 6, 2022; revised Apr. 19, 2023; accepted Apr. 21, 2023.

Author contributions: M.C., Y.C., C.J.W., D.H.G., and J.W.F. designed research; M.C., Y.C., V.P., A.C., and V.S. performed research; Y.C. and V.P. contributed unpublished reagents/analytic tools; M.C., Y.C., V.P., A.C., C.J.W., D.H.G., and J.W.F. analyzed data; M.C., Y.C., V.P., A.C., P.J., V.S., C.J.W., D.H.G., and J.W.F. edited the paper; M.C., Y.C., and J.W.F. wrote the paper.

*M.C. and Y.C. contributed equally to this work.

This work was supported by Medical Research Council Grants MR/R004544/1 and MR/R004463/1; the Netherlands Organization for Scientific Research Grant 013-16-002; Fight for Sight Grants 5065/5066, 5119/5120, and 5123/5124; the Wings for Life (WFL) Grant GB-04/19; the Czech Ministry of Education Grant CZ.02.1.01/0.0/0.0/15_003/0000419; ERA-NET NEURON AxonRepair; International Foundation for Research in

Paraplegia P172; the National Institutes of Health Grant R35NS105076; and the Dr. Miriam and Sheldon G. Adelson Medical Research Foundation.

The authors declare no competing financial interests.

Correspondence should be addressed to James W. Fawcett at jf108@cam.ac.uk.

<https://doi.org/10.1523/JNEUROSCI.2076-22.2023>

Copyright © 2023 Cheah, Cheng et al.

This is an open-access article distributed under the terms of the Creative Commons Attribution 4.0 International license, which permits unrestricted use, distribution and reproduction in any medium provided that the original work is properly attributed.

Introduction

Regeneration of axons in the damaged CNS is a currently unfulfilled requirement for the repair of damage to the nervous system. For successful regeneration, centrally projecting neurons need to be modified to enhance their intrinsic regenerative ability, and their properties need to be matched to the environment through which their axons must grow. How this interplay between extrinsic signals and intrinsic neuronal states is represented in genome-wide transcriptional programs is not well understood, and such an analysis requires a model in which there is extensive regeneration of axons in the CNS.

When the peripheral axon branch of sensory neurons is cut, the axons start to regenerate and a set of genetic and epigenetic changes occur in the cell body leading to the transcriptional upregulation of regeneration-associated genes (RAGs; Chandran et al., 2016; Curcio and Bradke, 2018; Rozenbaum et al., 2018; Palmisano et al., 2019; Renthal et al., 2020). Expression of this peripheral nervous system (PNS) regeneration program after a conditioning peripheral nerve lesion can enable some sensory axon regeneration in the spinal cord (Neumann and Woolf, 1999; Chandran et al., 2016). However, cutting the central branch in the dorsal root or spinal cord does not initiate the RAGs program.

Recently an integrin-based strategy has enabled long-distance central sensory neuron regeneration in the adult rat spinal cord with functional recovery (Andrews et al., 2009; Cheah et al., 2016; Nieuwenhuis et al., 2018). These approaches are based on the knowledge that axons regenerate through the extracellular matrix (ECM), for which the main receptors are integrins. In the uninjured/developing and damaged CNS, the main integrin ligand in the ECM is tenascin-C (Rauch, 2004; Dobbertin et al., 2010). Yet, $\alpha 9 \beta 1$ integrin, the primary tenascin-C receptor is downregulated in neurons after development and not re-expressed after injury. Expression of $\alpha 9 \beta 1$ integrin by itself is not sufficient to enable regeneration because integrins are inactivated by Nogo-A and chondroitin sulfate proteoglycans (CSPGs; Andrews et al., 2009). However, the addition of an inside-out integrin activator, kindlin-1, equips sensory neurons with the ability for extensive regeneration in the spinal cord, overcoming the CSPG-induced deactivation of integrins (Cheah et al., 2016). Thus, $\alpha 9$ -kindlin-1 transduced neurons can regenerate their axons for long distances along the dorsal column of the spinal cord, making appropriate connections in the dorsal horn and enabling recovery of sensation and locomotion. However, the molecular programs that underlie this remarkable change in internal growth state because of extrinsic signaling are not well understood.

The present study was designed to study the mRNA profile of sensory neurons whose axons, driven by $\alpha 9$ integrin and kindlin-1, were regenerating in the spinal cord. We profiled the changes in mRNA expression in regenerating (dorsal root axotomized) and nonregenerating (nonaxotomized) sensory neurons expressing $\alpha 9$ integrin and kindlin-1 compared with axotomized and nonaxotomized GFP controls, neither of which regenerated. This data were subsequently compared with recent profiling studies of peripheral sensory regeneration (Chandran et al., 2016; Tedeschi et al., 2016; Renthal et al., 2020).

The expression profile of neurons expressing $\alpha 9$ -kindlin-1-GFP without axotomy, and therefore not regenerating their axons, showed a remarkable number of expression changes, including upregulation of almost all the mRNAs previously identified as RAGs. This profile represents the effects of

signaling from activated integrins in the absence of injury. Comparing this group with the CNS regeneration group that were transduced with $\alpha 9$ -kindlin-1-GFP with axotomy, we observed a CNS regeneration program of mRNAs that was exclusively associated with regeneration in the spinal cord. The groups of mRNAs upregulated in these regenerating neurons were related to ubiquitination, autophagy, endoplasmic reticulum (ER) casein kinases, transcriptional regulators, transport/trafficking molecules, signaling molecules. Overall, the study reveals a distinct CNS regeneration program of mRNAs expressed during integrin-driven regeneration of axons in the CNS.

Materials and Methods

Animal surgeries

All animal surgeries were conducted in accordance with the United Kingdom Animals (Scientific Procedures) Act 1986. In this study, adult two-month-old male Lewis rats were used. DRG virus injection was performed according to the protocol described (Cheah et al., 2017). The three viruses used in this study were AAV5-CMV-fGFP, AAV5-CAG- $\alpha 9$ -V5, and AAV5-CMV-kindlin1-GFP, and they were obtained from the previous integrin study (Cheah et al., 2016). Briefly, one microliter of the virus at a working titer of 2×10^{12} GC/ml was injected into the left C5–C8 DRGs using a custom-made 33-gauge needle syringe (Hamilton) with an infusion syringe pump (World Precision Instruments) at 0.1 μ l/min. For the groups of animals with crush injury, the left C5–C8 dorsal roots were crushed using a pair of Bonn forceps (Fine Science Tools) for 3 \times 10 s for each root. The animals were kept for eight weeks for recovery, and were culled by exposure to a rising concentration of CO₂. The virus-injected left C5–C8 DRGs were harvested for fluorescence-activated cell sorting (FACS). The spinal cords were fixed with 4% paraformaldehyde (PFA) for *post hoc* immunohistochemical analysis.

Fluorescence-activated cell sorting (FACS)

Harvested DRGs were dissociated by incubating with 0.2% collagenase (Sigma) and 0.1% trypsin (Sigma), followed by trituration and centrifugation (Cheah et al., 2016). After dissociation, the cells were kept in ice-cold FACS buffer containing 1% BSA (Sigma), 2 mM EDTA (Sigma), 10 mM Na₂CO₃ (Sigma), 15 mM HEPES (Invitrogen) in PBS at pH 7.4, and immediately proceeded to FACS. The FACS Aria III Flow Cytometer (BD Biosciences) was used for cell sorting. Dissociated rat nestin-GFP left C5–C8 DRG cells were used as positive control to adjust forward and side scatters for doublet discrimination and debris exclusion. To obtain a pure population of GFP-positive cells, 488-nm emission with 530/30 BP filter was used, coupled with 633-nm emission and 660/20 BP filter as negative control. GFP-sorted cells were kept in ice-cold RNAlater (Ambion) and then moved to -80° C for storage in preparation for RNA-seq library.

RNA-seq library preparation

RNA from FACS-sorted cells ranging from 3000 to 10,000 were isolated with the NucleoSpin RNA XS kit (Clontech) with on column DNase digestion according to the manufacturer's protocol. The SMART-Seq v4 Ultra Low Input RNA kit (Clontech) was used for library preparation. The cDNA was fragmented to 300 base pairs (bp) using the Covaris M220 (Covaris), and then the manufacturer's instructions were followed for end repair, adaptor ligation, and library amplification. The libraries were quantified by the Qubit dsDNA HS Assay kit (Invitrogen); library size distribution and molar concentration of cDNA molecules in each library were determined by the Agilent High Sensitivity DNA Assay on an Agilent 2200 TapeStation system. Libraries were multiplexed into a single pool and sequenced using a HiSeq2500 instrument (Illumina) to generate 69-bp pair-end reads. An average of ~ 60 million reads were obtained for each sample.

RNA-seq read alignment and processing

RNA-seq data were mapped to the reference genome (mm10/GRCm38) using STAR (Dobin et al., 2013). Aligned reads were sorted, and alignments mapped to different chromosomes were removed from the BAM

file using SAMtools (<http://www.htslib.org/>). Alignment and duplication metrics were collected using the PICARD tools functions CollectRnaSeqMetrics and MarkDuplicates respectively (<http://broadinstitute.github.io/picard/>). Total counts of read fragments aligned to candidate gene regions were quantified by Salmon (Patro et al., 2017). Genes with <10 read counts in over 80% of the samples were removed. Gene counts were log₂-transformed with a small pseudocount. Potential bias from gene length and sequencing depth was normalized using *cqn* R package (Hansen et al., 2012).

Differential gene expression

Principle component analysis (PCA) of the normalized expression data (first five PCs) was correlated with potential technical covariates, including sex, batch, aligning and sequencing bias calculated from STAR and Picard respectively. Differential gene expression was performed using limma (Ritchie et al., 2015) on normalized gene counts, including batch the first three PCs of aligning and sequencing bias as covariates: ~ Genotype*Condition + Batch + AlignSeq.PC1 + AlignSeq.PC2 + AlignSeq.PC3, in which Genotype indicates mice expressing $\alpha 9$ integrin/kindlin-1 or GFP as control, and Condition indicates mice with or without dorsal root crush. Differentially expressed genes (DEGs) were determined at FDR p -value < 0.1. K -means clustering ($n = 4$) were performed on genes that are upregulated by over-expressing $\alpha 9$ integrin/kindlin-1 with or without crush, which leads to gene clusters that are uniquely or commonly upregulated in either condition.

Rank–rank hypergeometric overlap

We performed a rank–rank hypergeometric test as previously described (Plaisier et al., 2010). Genes were ranked according to their logFC before running the rank–rank hypergeometric overlap (RRHO) test to evaluate overlap between two datasets.

Gene Ontology analysis

Gene Ontology (GO) term enrichment analysis was performed using the gProfileR package (Reimand et al., 2016), using expressed genes in each of the normalized dataset as background. Genes enriched in the top GO terms of interest ranked by FDR p -value < 0.05 were manually checked on Uniprot and PubMed for relevance. The very general terms were excluded, and terms with low p -values and potential relevance selected. GO terms with similar contents were gathered together.

Weighted gene co-expression network analysis

Sequencing and aligning covariates were regressed out from normalized expression data using a linear model. Co-expression network was constructed using the weighted gene co-expression network analysis (WGCNA) package (Langfelder and Horvath, 2008). Briefly, pair-wise Pearson correlations between each gene pair were calculated and transformed to a signed adjacency matrix using a power of 10, as it was the smallest threshold that resulted in a scale-free R^2 fit of 0.8. The adjacency matrix was used to construct a topological overlap dissimilarity matrix, from which hierarchical clustering of genes as modules were determined by a dynamic tree-cutting algorithm.

WGCNA module annotation

To classify upregulated or downregulated modules, the module eigengene, defined as the first principle component of a module that explains the maximum possible variability of that module, was related to genotype ($\alpha 9$ integrin/kindlin-1 vs GFP) using a linear model. Modules were considered to be significantly associated with the phenotype when Bonferroni-corrected p -values are <0.05. To annotate modules at a general level, we applied Gene Ontology (GO) enrichment analyses on each module. As a further step toward functional annotation, we performed hypergeometric analysis to examine each module's association with the regeneration-associated gene (RAGs) module known to be activated by peripheral injury (Chandran et al., 2016), or transport-associated gene module. Modules were considered to be significantly associated with each of the gene program when Bonferroni-corrected p -values are <0.05. The Pearson correlations between each gene and each module eigengene as a gene's module membership were also calculated, and hub genes were

defined as being those with highest correlations ($kME > 0.85$). The co-expression networks of these most central genes representing key biological pathways upregulated in the regenerating DRG neurons were plotted using *igraph* R package (<https://igraph.org/r/>). Correlations of ME between DEG clusters and WGCNA modules were calculated using *bicor()* in the WGCNA package and bi-weighted mid-correlation (R) values were plotted in a multidimensional scaling plot.

Transcription factor enrichment analysis

Enrichr (Chen et al., 2013; Kuleshov et al., 2016) was used to predict the upstream transcription factors of each WGCNA modules using position weight matrices (PWMs) from TRANSFAC and JASPAR scanning the promoters of genes in the region between –2000 and +500 of a gene's transcription start site. This workflow also integrates existing ChIP-seq data from ENCODE (Rosenbloom et al., 2012) and ChEA (Lachmann et al., 2010). The TF-target network containing predicted TFs and module genes predicted to be bound by each TF was plotted using *igraph*.

Ubiquitination network analysis

UbiNet (Nguyen et al., 2016) was used to search for ubiquitination networks and hubs among mRNAs expressed in the magenta/black/turquoise modules. The upregulated genes were submitted to the UbiNet Network Analysis platform to identify the potential E3 ligase-substrate interactions. The most interacted E3 ligases or hubs were selected, with their cellular functions cross-checked manually on UniProt and PubMed.

Immunohistochemical analysis

Sections of PFA-fixed spinal cords were cut at 14 μm on a cryostat and blocked in 0.4% Triton X-100 (Sigma) and 10% normal goat serum (Invitrogen). The tissues were then incubated with primary antibodies overnight at 4°C and secondary antibodies for 2 h at room temperature. Primary antibodies used were rabbit anti-GFP (1:500; Invitrogen A-11122) and mouse anti-V5 (1:250; Invitrogen R963-25); secondary antibodies were Alexa Fluor 488 and 568 (1:500; Invitrogen).

DRG explant neurite regeneration assay

Cervical DRGs from two-month-old male Wistar rats were isolated with connective tissues removed. Each DRG was trimmed into two to four pieces and plated on μ -Slide angiogenesis chamber slides (Ibidi) coated with poly-D-lysine (20 $\mu\text{g}/\text{ml}$; Sigma) and laminin (10 $\mu\text{g}/\text{ml}$; Sigma). The culture media were refreshed daily to promote neurite outgrowth. On day 5, inhibitors were added to the media and incubated for 1 h before axotomy. The inhibitors used were: NSC697923 (0.3 μM , Tocris Bioscience), MLN4924 (5 μM , Tocris Bioscience), MG132 (10 μM , Abcam), 3-Methyladenine (2.5 mM, Abcam), and D4476 (10 μM , Tocris Bioscience). To perform axotomy, a glass pulled pipette was used to leave a clear demarcation on the slides. The tissues were returned to the incubator for 2 h after axotomy. Images were taken immediately after axotomy and at 2 h using the Axio Observer D1 Inverted Phase Contrast Microscope (Zeiss). Analysis was performed using ImageJ by quantifying the number of regenerating neurites.

Human iPSC-derived sensory neuron regeneration assay

Human induced pluripotent stem cell (iPSC)-derived sensory neurons were generated in a collaboration with Ilyas Singec's group at the National Center for the Advances of Translational Sciences (NCATS) at the NIH (Patent Publication Number: WO/2020/219811; Singec et al., 2020; Deng et al., 2023). In short, human iPSCs were cultured until 70–80% confluent, treated with a combination of small molecule inhibitors and grown into neurospheres for 14 d. Neurospheres were then dissociated and replated as individual spot cultures on 24-well plates. Each spot contained 60,000 cells and was further matured for 21 d until long axons protrude out of the spot. On day 35 days in vitro (DIV), cells were treated with inhibitors 2 h before laser axotomy was performed with a 300-mW Stiletto infrared laser (Hamilton Thorne) combined with a 20 \times objective as described previously (Ho et al., 2021). The laser module has a high-speed micro controller and an automated motorized stage. Axons were cut around 400–600 μm away from the cell bodies. Spots were imaged before and every 2 h for up to 24 h after

cut using the live-cell imaging system – IncuCyte S3 (Satorius). Images were extracted from the IncuCyte software and areas of interest were cropped to include the regenerating processes and injury site. Images were then converted into eight-bit images in Fiji ImageJ and Sholl analysis was performed at every micron for 250 μm away from the injury site at different time points; % regeneration was measured by the total number of processes at time \times after cut/total number of processes before cut. The inhibitors used were: NSC697923 (0.3 μM , Tocris Bioscience), MLN4924 (5 μM , Tocris Bioscience), MG132 (10 μM , Abcam), 3-Methyladenine (0.5 mM, Abcam), and D4476 (10 μM , Tocris Bioscience).

Accession numbers

The accession numbers for the data generated in this paper are GSE188775 and GSE188776.

Results

Four experimental groups of adult male Lewis rats were created through injection of either AAV5-fGFP or AAV5- $\alpha 9$ -V5 + AAV5-kindlin1-GFP into four cervical (left C5–C8) dorsal root ganglia (DRGs) with and without dorsal root crush. The groups were: (1) $\alpha 9$ -kindlin-1-GFP with dorsal root crush to enable axon regeneration in the spinal cord ($\alpha 9$ k1-crush), (2) $\alpha 9$ -kindlin-1-GFP with no axotomy and therefore no regeneration to examine the effects of activated integrin expression without regeneration ($\alpha 9$ k1-naive), (3) GFP with axotomy to control for the effects of AAV injection and axotomy without regeneration (GFP-crush), and (4) GFP with no axotomy to control for the effects of AAV injection (GFP-naive). The DRGs were removed after eight weeks, at which time many axons are actively regenerating in the spinal cord, and GFP-expressing neurons were dissociated and selected by fluorescence-activated cell sorting (FACS), then mRNA purified and profiled by sequencing (timescale in Fig. 1A).

Expression of integrin and kindlin drives sensory regeneration into the spinal cord

In previous work, we showed that expression of $\alpha 9$ integrin and kindlin-1 enables extensive sensory axon regeneration in the spinal cord (Cheah et al., 2016). Here, we confirmed this result in a pilot experiment, examining axon growth at the same time point as the RNA extractions, to be sure that we were extracting RNA from neurons with axons actively regenerating in the spinal cord. The left C5–C8 dorsal root ganglia (DRGs) were injected with either AAV5-fGFP or AAV5- $\alpha 9$ -V5 + AAV5-kindlin1-GFP. Concurrently during virus injection, the left C5–C8 dorsal roots in half of the animals were crushed. Animals were sacrificed after eight weeks and sensory projections in the spinal cord were examined. Axons from the DRGs were traced using GFP alone or kindlin-1-GFP. In the spinal cord of $\alpha 9$ k1-crush animals, many regenerated axons were seen in the dorsal columns with terminals in the dorsal horn (Fig. 1B–D) as observed previously. This replicates our previous regeneration experiment (Cheah et al., 2016). In the GFP-crush animals, there was no regeneration into the spinal cord (Fig. 1E). In addition, the spinal cords in the $\alpha 9$ k1-naive group were examined to determine whether expression of $\alpha 9$ +kindlin-1 caused abnormal sprouting of axons or terminals. This analysis showed that there was no abnormal sprouting of axons in the dorsal columns, and the projections in the dorsal and ventral horns showed no signs of aberrant sprouting, with no processes projecting beyond the central gray matter and no midline crossing (Fig. 1F,G). Expression of $\alpha 9$ integrin and kindlin-1 was therefore sufficient to enable extensive regeneration of crushed central sensory axons into the spinal cord, but it did not cause abnormal

sprouting of uncut axons. A schematic summary of the design and results of the current *in vivo* regeneration study, and our previous results, is shown in Figure 1H. The DRGs treated in these experiments were C5–C8, so our study does not address potential differences between cervical and lumbar sensory neurons (Lallemend et al., 2012; Golan et al., 2021).

Transcriptional changes

DRGs were harvested eight weeks after virus injection and dorsal root crush, timed to coincide with ongoing axon regeneration. An example of $\alpha 9$ integrin and kindlin-1 co-transduced DRG is shown in Figure 2A, with a co-transduction rate of 75%. The co-transduction level for this study was very similar to our previous study at 80%. After tissue collection, DRGs were dissociated into single cells, and then GFP-expressing or kindlin-1-GFP-expressing neurons were selected by FACS (Fig. 2B). *Post hoc* sampling showed FACS-sorted cells contained both large and small DRG neurons by co-staining with NF200 or CGRP, respectively (Fig. 2C).

Transcriptomic analysis via RNA-seq was performed using four to six biological replicates for each condition (Materials and Methods). Comparison of differentially expressed genes between the GFP and $\alpha 9$ k1 groups (Materials and Methods) revealed that among the most upregulated mRNAs were kindlin-1 (FERMT1, log₂FC = 6.46) and $\alpha 9$ integrin (ITGA9, log₂FC = 5.69), shown in volcano plots in Figure 3A, demonstrating that AAV transduction for expression of $\alpha 9$ integrin and kindlin-1 had been successful and validating the sorting and sequencing methods. The numbers of differentially expressed genes in the experimental groups are shown in Figure 3B, and the quantitation of overlapping genes in Figure 3C.

Analysis of transcriptional changes by clusters and modules

In our analysis, 2443 genes were upregulated by integrin-kindlin expression, with or without dorsal root crush, compared with GFP controls [false discovery rate (FDR) of $p < 0.1$; Fig. 3B]. To identify genes associated with CNS axon regeneration ($\alpha 9$ k1-crush, the regeneration group), we applied *K*-means clustering, identifying four clusters, which are visualized on a combined expression heatmap (Fig. 4) and shown as individual clusters (Fig. 5). Cluster 1 contains genes upregulated in neurons transduced with $\alpha 9$ k1 in combination with central axotomy, many of which were regenerating their axons into the spinal cord (CNS regeneration program). Of these 66% are elevated only in the $\alpha 9$ k1-crush group and 19% are elevated in both the $\alpha 9$ k1-naive and $\alpha 9$ k1-crush compared with the GFP-naive group by log₂FC (Fig. 3). Cluster 2 contains genes upregulated by $\alpha 9$ k1 expression without dorsal root crush, but not upregulated in the regeneration group (isolated $\alpha 9$ k1 program). Cluster 3 contains genes upregulated in both the $\alpha 9$ k1-naive and $\alpha 9$ k1-crush groups (mixed $\alpha 9$ k1 program), and Cluster 4 contains genes upregulated by dorsal root crush without $\alpha 9$ k1 expression, and therefore without any regeneration (injury program).

To further refine our analysis by identifying networks of highly co-expressed genes we performed weighted gene co-expression network analysis (WGCNA) of the entire dataset, identifying 11 distinct modules (Fig. 6A), named by colors as per convention (Langfelder et al., 2008). Based on the correlation of the first principal component (PC1) of a module (module eigengene) with treatment (Materials and Methods; Fig. 6B), we found that the magenta, black, and green modules were more positively associated with the $\alpha 9$ k1-crush (CNS regeneration) group, while the turquoise and tan modules

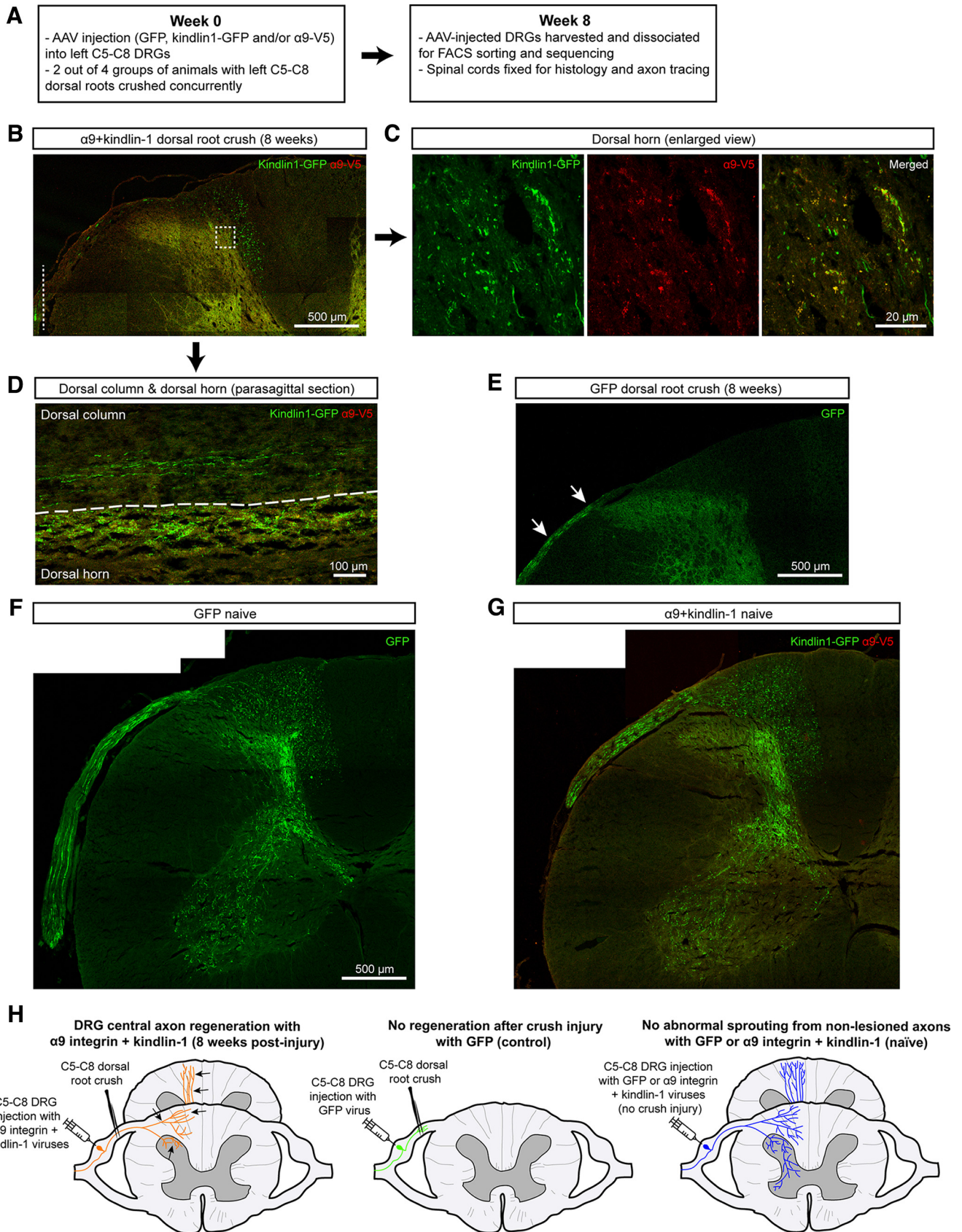


Figure 1. Axonal regeneration with no abnormal sprouting in the spinal cord. **A**, Time course of the experiment. **B–G**, Results from the replication pilot experiment performed in this study. A full set of results is shown in our previous paper (Cheah et al., 2016). **B–D**, Regenerated axons (**B**) in transverse section in the dorsal column and dorsal horn of an $\alpha 9$ k1-crush animal. The white dotted line in **B** indicates the crush site. **C**, Magnified square outlined in **B**. **D**, Regenerated axons and their terminals in gray matter in the dorsal column and dorsal horn in a parasagittal section. **E**, For the GFP-crush animal, GFP-labeled axons (white arrows) are seen in the dorsal root but none have regenerated into the spinal cord. **F**, **G**, Sensory projections of unlesioned animals, GFP-naïve (**F**) and $\alpha 9$ k1-naïve (**G**). There was no abnormal sprouting of axons that contain activated integrin, and no processes are seen sprouting from gray to white matter. **H**,

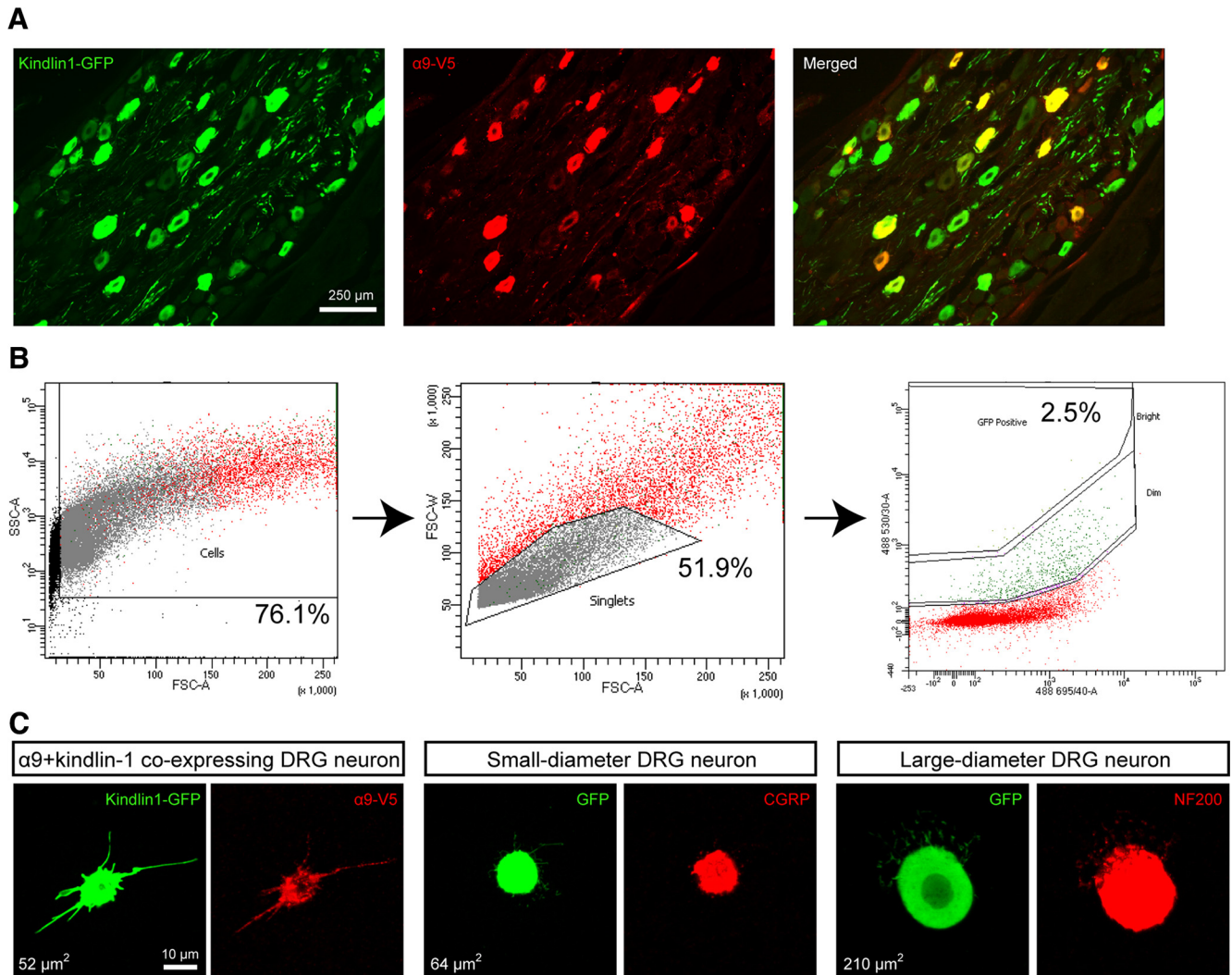


Figure 2. Immunostaining and FACS sorting of $\alpha 9$ integrin and kindlin-1-expressing DRG neurons. **A**, A typical section from a DRG injected with $\alpha 9$ integrin and kindlin-1 viruses, with 75% co-transduction. **B**, The multigated approach of sorting dissociated GFP-expressing DRG neurons using the BD Aria III Flow Cytometer. Dissociated rat nestin-GFP left C5–C8 DRG cells were used as positive control to adjust forward and side scatters for doublet discrimination and debris exclusion. A pure population of single dissociated GFP-expressing DRG neurons, $\sim 2.5\%$ of the total cell population, was obtained. **C**, A small sample of sorted DRG neurons were cultured and analyzed for $\alpha 9$ integrin and kindlin-1 co-expression, and co-stained with CGRP or NF200 for verification.

were positively associated with the mixed $\alpha 9k1$ program and the pink module was positively associated with the $\alpha 9k1$ program. The relationships of the modules to the various treatment and injury groups (eigengene correlations) are shown in Figure 6C for magenta, black, green, turquoise, tan, pink, blue, and purple modules, and in Figure 6D for other modules not relevant to our subsequent analyses.

The blue module contained mRNAs that were downregulated in the GFP-crush and $\alpha 9k1$ -crush groups, whereas the purple module contained mRNAs that were downregulated in the $\alpha 9k1$ -crush group (Fig. 4C). In the blue module, relevant Gene

Ontology (GO) terms were cell motility ($p = 0.0003$), cell adhesion ($p = 0.001$), cell surface receptor signaling ($p = 0.001$). In the purple module, there were only two GO terms containing 12 genes which are not relevant to axon regeneration. Examination of the genes included in the blue module revealed downregulation of mRNAs associated with Wnt and Notch signaling (Wnt6, Wnt11, Fzd3, Ryk, Notch1, Notch4, and Jag1). Both the Wnt and Notch pathways are inhibitory to axon regeneration and suppression of Wnt and Notch signaling has promoted regeneration (El Bejjani and Hammarlund, 2012; Onishi et al., 2014; van Vliet et al., 2021).

Comparison of the clusters and modules by similarity network analysis showed that there was a close correlation between the magenta module and Cluster 1, the turquoise module and Cluster 3 (Fig. 6E). A general GO analysis did not find relevant biological processes associated with the tan and green modules. The magenta, black, pink, and turquoise modules and equivalent clusters were examined in more detail since they appeared to represent coherent biological processes relevant to our treatment paradigm and axon regeneration.

←

Schematic summary of the design and main outcomes of the study. The schematic represents the results from our previous sensory regeneration study, replicated in the pilot experiments illustrated in B–G. In the left-hand diagram, $\alpha 9$ integrin and kindlin-1 AAVs have been injected into DRGs and their dorsal roots crushed; regenerating axons (black arrows) are present in the dorsal columns. The middle diagram shows the absence of regeneration after injection of AAV-GFP into DRGs combined with dorsal root crush. The right-hand diagram shows the normal sensory projection in unlesioned animals expressing integrin/kindlin.

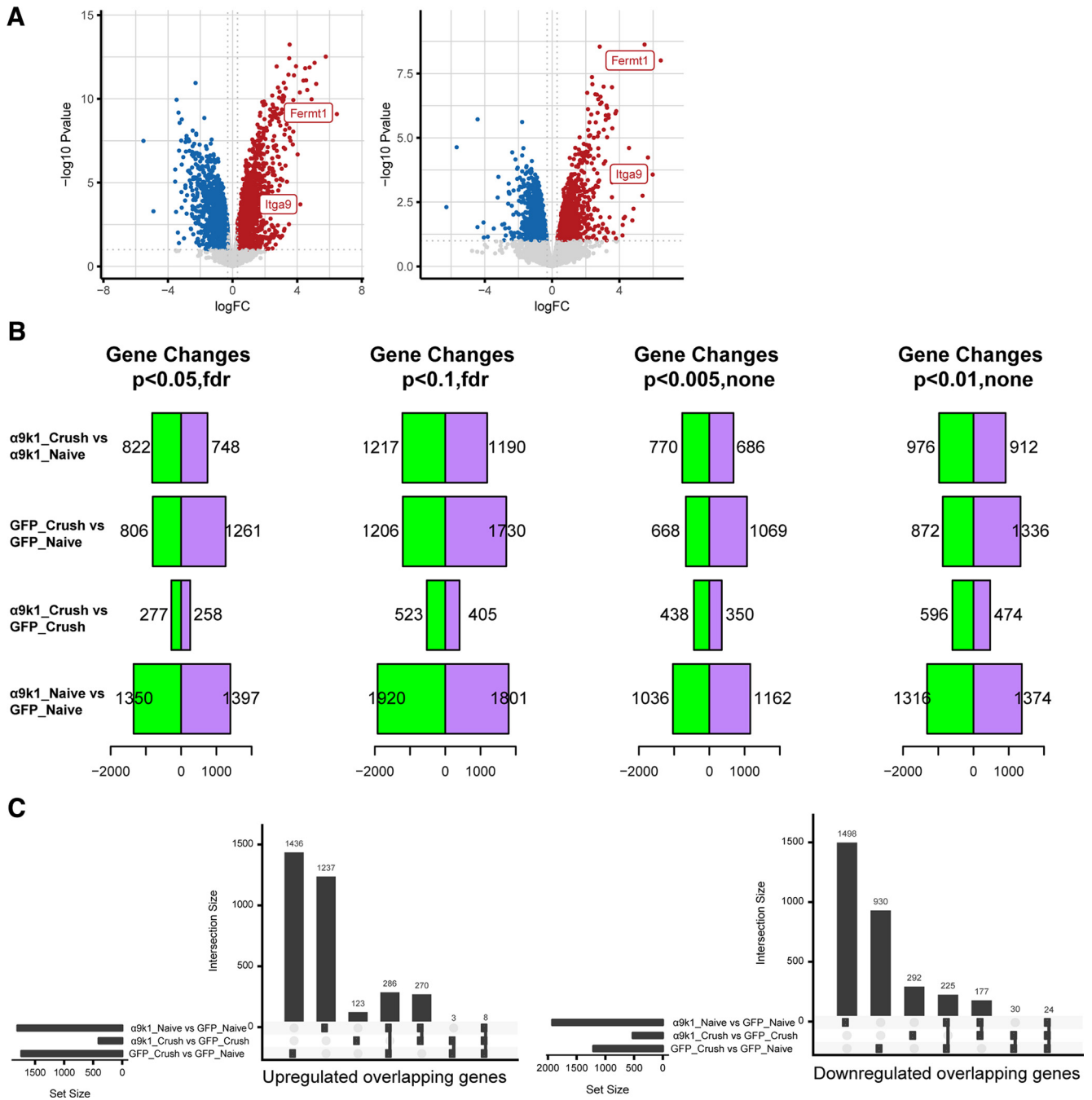


Figure 3. Differential expression between experimental and control groups. **A**, Volcano plots showing the high expression levels of kindlin-1 (*Fermt1*; log2FC = 6.46; left) and $\alpha 9$ integrin (*Itga9*; log2FC = 5.69; right) in transduced sensory neurons. **B**, The number of differentially expressed genes at different *p*-values in different experimental and control groups: $\alpha 9k1$ -crush versus $\alpha 9k1$ -naive, GFP-crush versus GFP-naive, $\alpha 9k1$ -crush versus GFP-crush, and $\alpha 9k1$ -naive versus GFP-naive. The false detection rate (FDR) *p*-value < 0.1 was selected to determine the number of differentially expressed genes (DEGs). **C**, Quantitation of upregulated (left) and downregulated (right) overlapping genes from **B**.

The GO of the clusters and the relevant modules were determined (Figs. 5, 7). Genes in GO terms of interest ranked by FDR-corrected *p*-value were manually curated to select transcripts of potential relevance. Similar GO terms were combined in Figure 5C–E and in the tables in the Extended Data Figures 7-1 and 7-2 attached to Figure 7. The black and magenta modules contain genes associated with axon regeneration (Fig. 7A), while the turquoise and pink modules contain genes upregulated by integrin signaling (Fig. 7B). We have kept black-magenta and turquoise-pink separate because GO analysis showed them to contain distinctive genes and functions.

A distinctive set of transcripts representing a CNS regeneration program was upregulated only in the $\alpha 9k1$ -crush condition (CNS regeneration group), seen in Cluster 1 and the magenta and black modules (Figs. 5C, 6B,C). The most significant GO terms included signaling, protein ubiquitination, autophagy, endomembrane system organization, transport/trafficking/localization, vesicle organization, and cytoskeletal protein binding (Figs. 5C, 7A). A different set of transcripts was associated with expression of $\alpha 9k1$ with or without dorsal root crush (mixed and isolated $\alpha 9k1$ programs). These genes appear in Clusters 2 and 3 and in the pink and turquoise modules (Figs. 5D,E, 7B) and

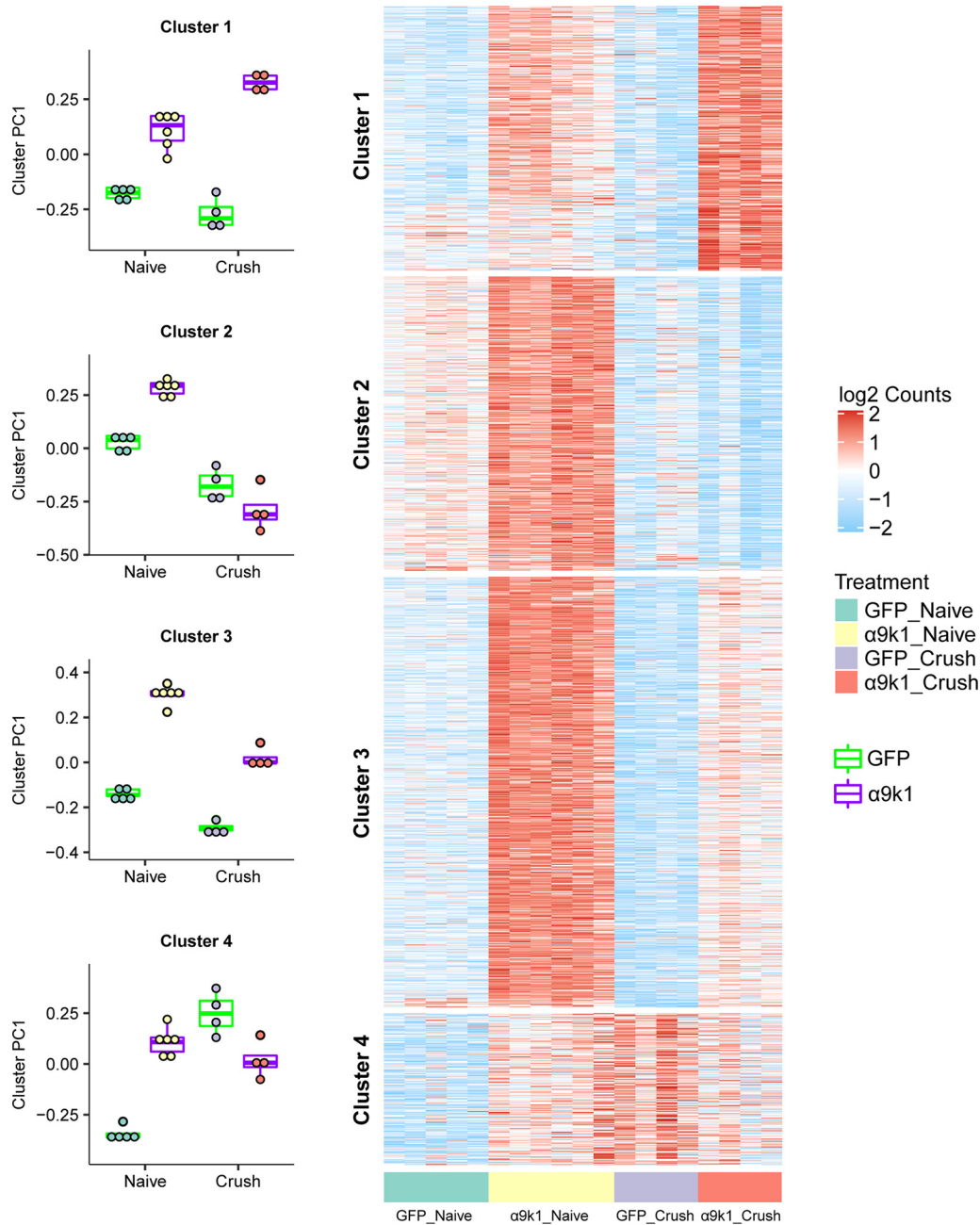


Figure 4. Clustering of genes upregulated by $\alpha 9k1$ expression. *K*-means clustering was applied to genes differentially upregulated comparing $\alpha 9k1$ -naive to GFP-naive, or comparing $\alpha 9k1$ -crush to GFP-crush (FDR p -value < 0.1). These genes are divided into four clusters: Cluster 1 is associated only with $\alpha 9k1$ -driven axon regeneration, Cluster 2 is associated with $\alpha 9k1$ expression, Cluster 3 is associated with $\alpha 9k1$ expression and sensory axon regeneration, and Cluster 4 is associated with crush injury alone. Principal component analysis (PCA) was performed on each gene cluster. The boxplot shows the first PC (PC1), which accounts for the largest variance of gene expression changes against treatment. These plots give a statistical analysis of the association between the four clusters and the experimental groups in the experiment. Expression levels (\log_2 normalized, row scaled) of individual genes from each cluster were visualized by a heatmap.

represent immune processes, cytokine production, transcriptional regulation, biological adhesion, signaling, and ubiquitin-protein transferase activity. Gene networks of these genes and their curated terms are shown in Figure 7A,B. To visualize interactions between the selected genes, network interaction diagrams were made for the hub genes ($kME > 0.85$) enriched in black/magenta (Fig. 7A) module GO terms and for the pink/turquoise gene networks (Fig. 7B). These networks reveal a rich set of interactions that couple the biological processes related to $\alpha 9k1$ signaling in distinct patterns depending on their relationship to central sensory axon regeneration in the spinal cord.

Expression of integrin and kindlin upregulates the PNS regeneration program

Analysis of the expression level clustering and co-expression network module analyses were performed to examine correspondence between transcripts in Clusters 2, 3 and the pink and turquoise modules that were upregulated by $\alpha 9k1$ expression (Figs. 5D,E, 7B). Cluster 2 includes mRNAs related to cell adhesion, integrin binding, and signaling (Fig. 5D). Cluster 3 GO terms of interest include actin skeleton, early endosomes, inflammatory immune response, MAPK cascade, and transcription factors (Fig. 5E).

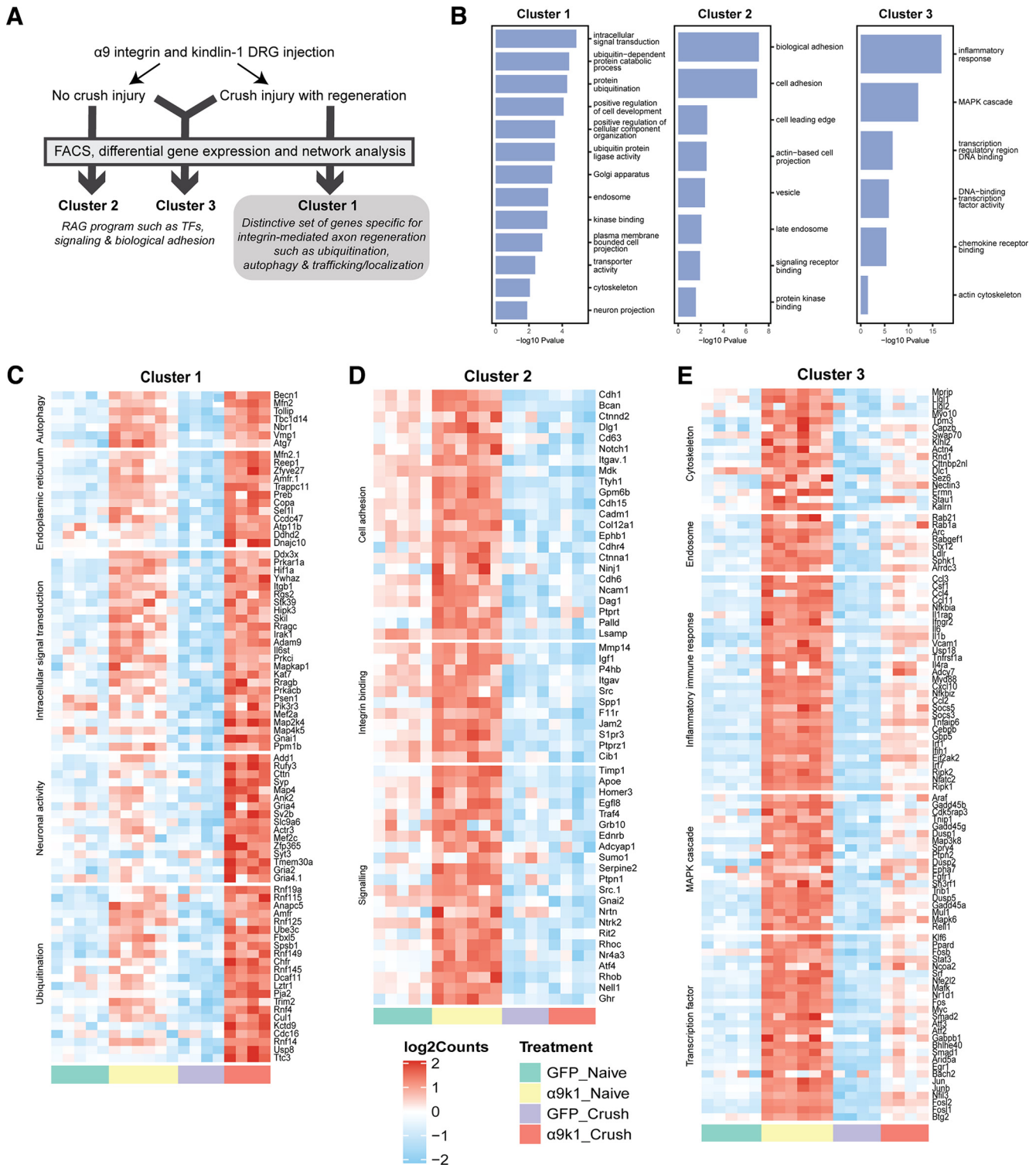


Figure 5. Individual heatmaps with relevant GO terms from Clusters 1, 2, and 3. **A**, Summary of the experimental groups and gene clusters. **B**, Top GO terms of interest ranked by *p*-value for Clusters 1–3 using GO terms with an enrichment FDR < 0.05. Genes enriched in the top GO terms were manually checked on UniProt and PubMed for relevance. **C**, Cluster 1 genes upregulated specifically in the α9k1-crush group (red bar) with relevant GO terms such as autophagy, endoplasmic reticulum, intracellular signal transduction and ubiquitination. **D**, Cluster 2 genes upregulated in the α9k1-naive group (yellow bar) with relevant GO terms such as cell adhesion, integrin binding and signaling. **E**, Cluster 3 genes upregulated in α9k1 groups with or without crush injury (red and yellow bars); relevant GO terms include cytoskeleton, endosome, inflammatory response, MAPK cascade and transcription factor.

The transcription factor term in Cluster 3 is of particular interest since it contains many of the traditional regeneration-associated molecules (RAGs), including the recognized transcription factor RAGs Klf4, Klf6, Jun, Myc, Atf3, Egr1, Egr2, Smad1, Stat3, Fos, Fosl1, Fosl2, and Cebp. A larger list of regeneration-related

mRNAs was identified previously (Chandran et al., 2016; Chandran RAGs list). Many of these appear in Cluster 3 and pink and turquoise modules in the transcription factor, inflammation and signaling GO terms [transcripts that appear in our Cluster 3, pink and turquoise, and also in

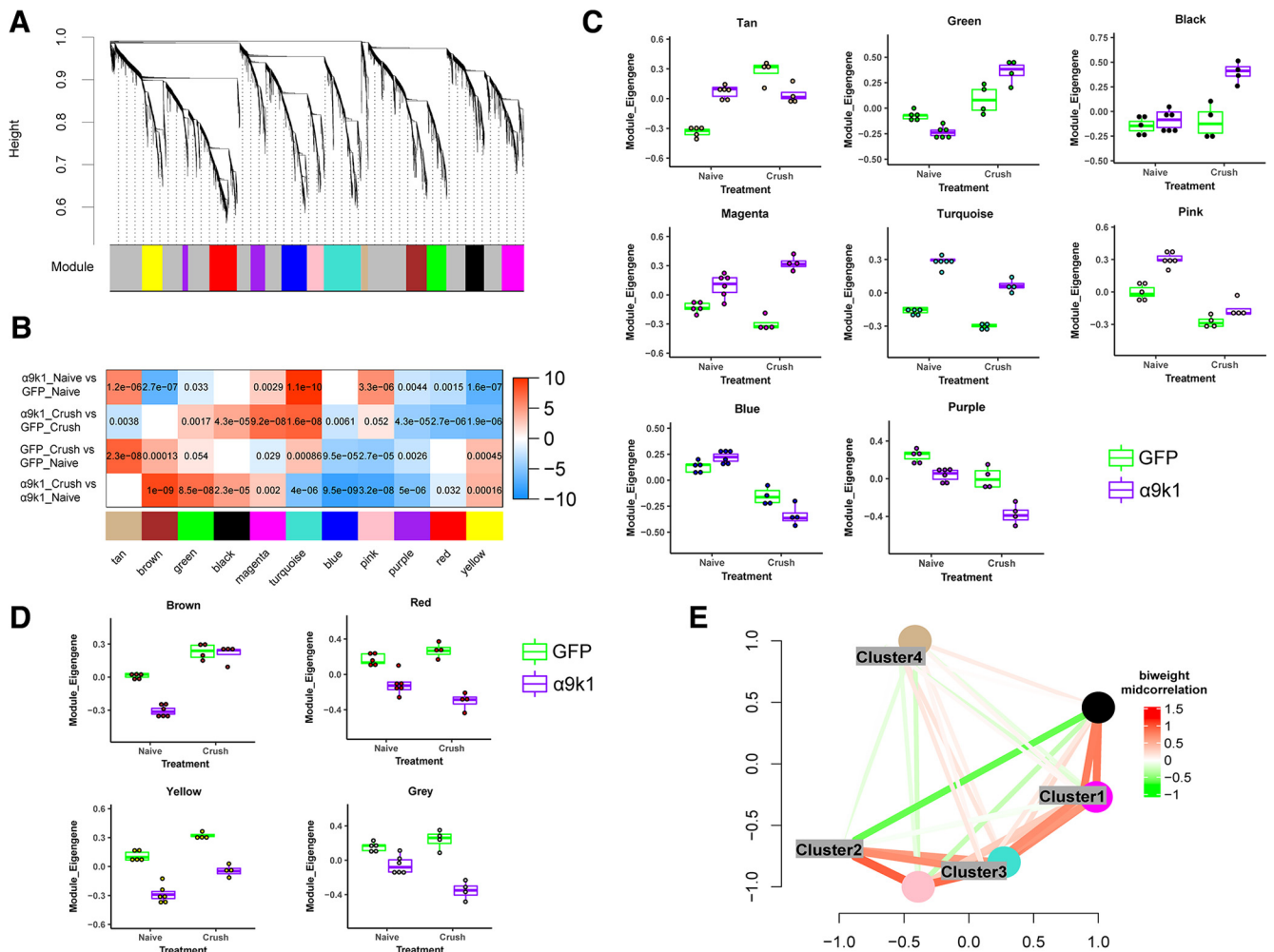


Figure 6. WGCNA of the dataset showing different expression patterns of the modules. **A**, Dendrogram showing the values that enabled identification of 11 WGCNA modules. **B**, Correlation between module eigengenes and the experimental groups. The first principle component driving the expression changes of a module is plotted against with treatment groups. In the correlation heatmap, colors indicate $-\text{sign}(\text{correlation coefficient}) \times (\log_{10} p\text{-value})$. Red indicates a positive correlation and blue indicates a negative correlation. Numbers shown are Bonferroni-corrected p -values. Green, magenta, and black modules were more associated with the $\alpha 9k1$ -crush (regeneration) group, while tan, turquoise, and pink modules were more associated with the $\alpha 9k1$ -naive group. **C**, Statistical analysis of the correlation between modules and experimental groups. Trajectory of the module eigengene is shown across treatment and control groups for tan, green, black, magenta, turquoise, pink, blue, and purple modules. **D**, Brown, red, yellow, and gray modules did not show correlations to any specific experimental groups of interest, hence not considered for subsequent analyses. **E**, Multidimensional scaling plots showing correlations between module eigengenes of the WGCNA modules and DEG clusters. Colors indicate bi-weighted mid-correlation (R) values. This analysis demonstrates similarities between Cluster 1 and magenta, Cluster 3 and turquoise.

Chandran et al. (2016), RAGs modules are highlighted in green in Extended Data Fig. 7-2].

Given this overlap, we next asked whether the integrin-driven changes resemble those that occur during PNS regeneration. Over-representation analysis revealed a strong correlation between the pink and turquoise modules and genes upregulated during PNS regeneration in a previous study (Chandran et al., 2016; Fig. 8A). A correlation analysis using rank–rank hypergeometric overlap (RRHO) heatmaps compared the logFCs of the experimental groups versus GFP controls, and a study (not previously published) of mRNA changes after sciatic nerve crush, comparing DRG neurons FACS-purified 1 and 5 d after axotomy with controls (GSE188776). There was a strong correlation between changes in the $\alpha 9k1$ -naive group and changes after PNS axotomy (Fig. 8B). Dorsal root crush injury alone, comparing the GFP-naive with the GFP-lesion group did not upregulate any of these factors. These findings indicate that signaling downstream of activated integrins is sufficient to activate a regeneration program. This regeneration program leads to a pattern of

mRNA expression that closely resembles that caused by peripheral nerve axotomy and subsequent regeneration, and includes most of the major recognized RAGs.

Spinal cord regeneration is associated with upregulation of a CNS regeneration program

A distinct set of genes was associated only with the $\alpha 9k1$ -crush (CNS regeneration) group. We observed that most of the genes described above that were upregulated in the $\alpha 9k1$ -naive group, many of which were recognized RAGs such as *Atf3*, *Myc*, *Fos1*, *Stat3* also remained upregulated in the $\alpha 9k1$ -crush group (Fig. 4). However, we observed another set of genes specifically upregulated only in the $\alpha 9k1$ -crush group. These transcripts were found in Cluster 1 (Fig. 5C), and in the magenta and black modules (Fig. 6B,C). Gene ontology analysis of these clusters and modules shows that many of these genes are enriched in biological processes related to autophagy, ubiquitination, endoplasmic reticulum and signaling (Figs. 5C, 7A), which were involved in most of the top GO terms. Transcripts curated for relevance are

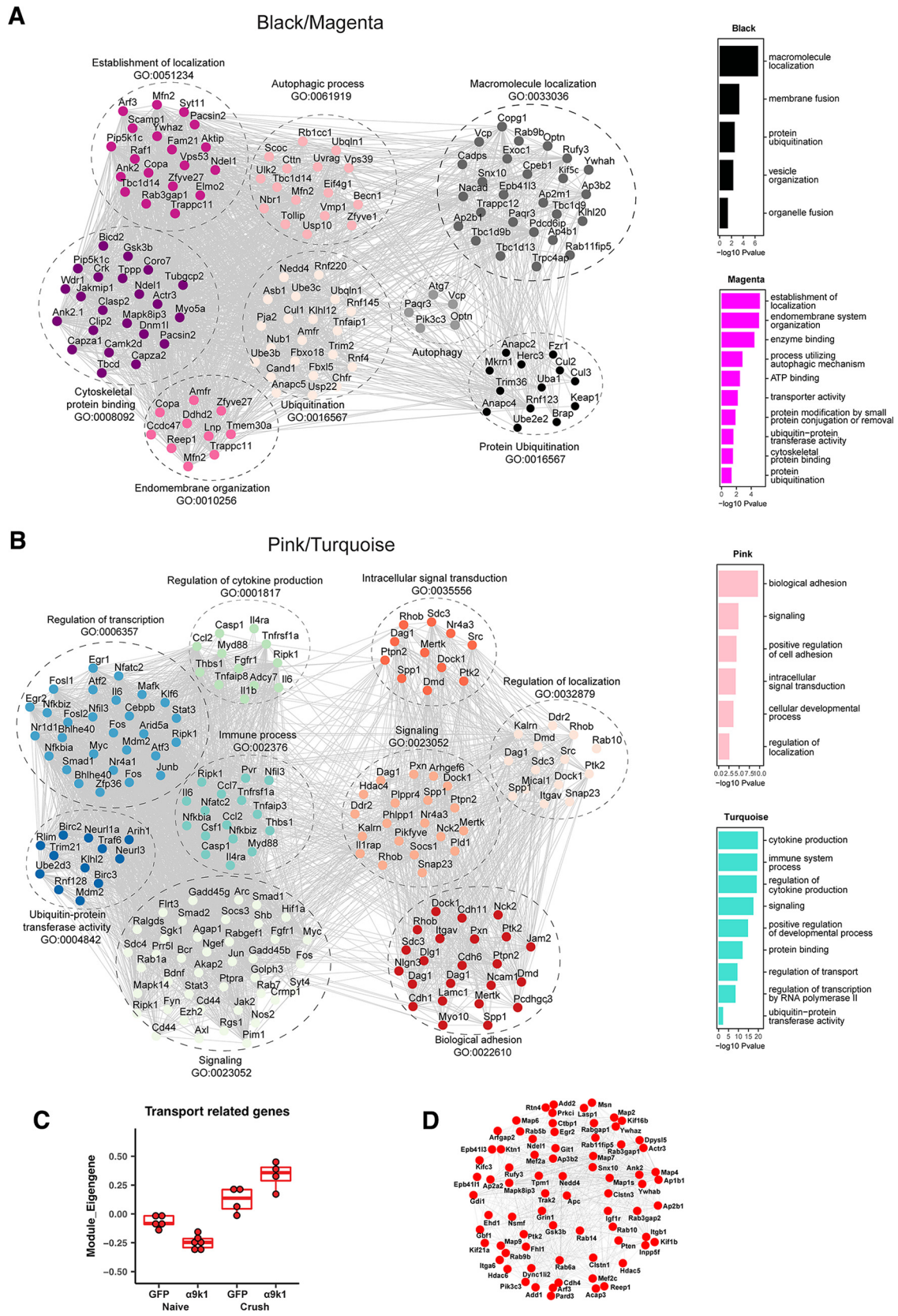


Figure 7. Gene co-expression networks of pink/turquoise and black/magenta modules. GO analysis was performed for the magenta/black modules associated with $\alpha 9k1$ -driven axon regeneration and the pink/turquoise modules associated with $\alpha 9k1$ expression. Co-expression networks were plotted for top-ranked related GO terms. The GO term analysis for each of black, magenta, pink and turquoise modules are shown on the side, ranked by p -value using GO terms with an enrichment FDR < 0.05. Genes enriched in the top GO terms were manually checked on UniProt and Pubmed for relevance. Information on the individual genes and GO terms is shown in Extended Data Figure 7-1 for Cluster 1, magenta and black modules for the $\alpha 9k1$ -crush (regeneration) group and Extended Data Figure 7-2 for Clusters 2 and 3, pink and turquoise modules for the $\alpha 9k1$ -naive group. **A**, The GO analysis of the $\alpha 9k1$ -regeneration-related magenta/black modules revealed that genes related to ubiquitylation, autophagy, and endomembrane organization (with many endoplasmic reticulum-related molecules) had a high level of

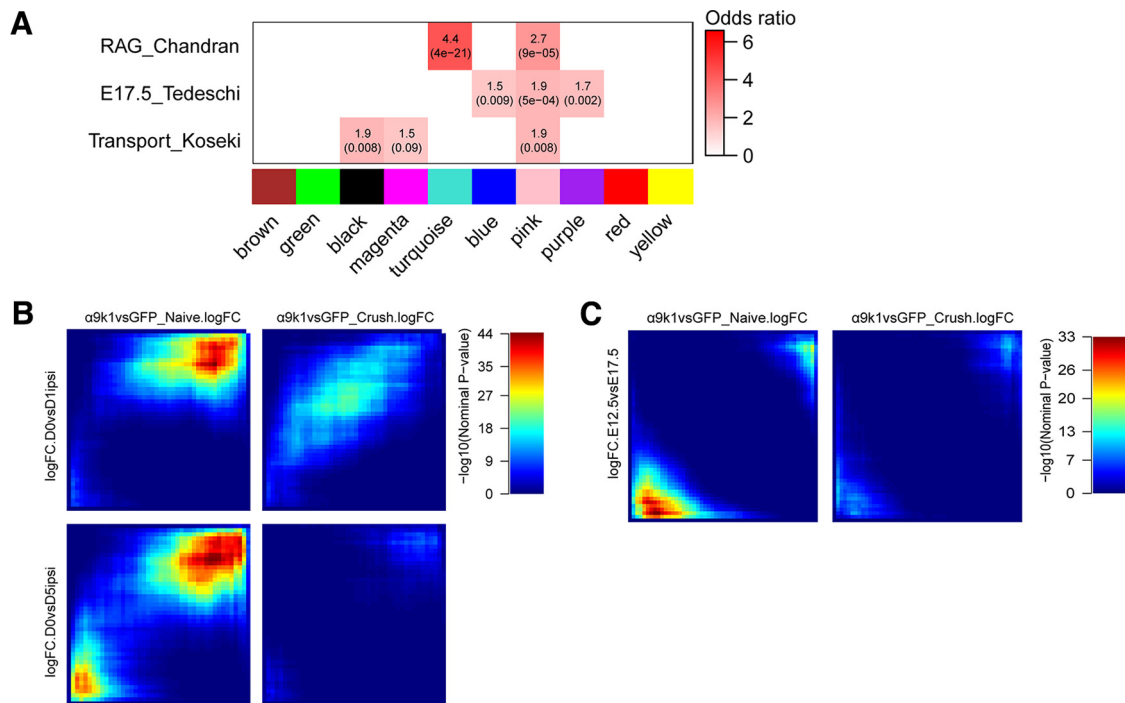


Figure 8. Correlations with PNS regeneration and development. **A**, Gene overlap analysis was performed to determine whether modules regulated by $\alpha 9k1$ are enriched with known gene signatures previously published. Comparisons are between a gene set activated during peripheral nerve regeneration (RAG_Chandran; Chandran et al., 2016), genes associated with DRG neuronal development (E8_Tedeschi; Tedeschi et al., 2016), or the genes associated with neuronal trafficking (Transport_Koseki; Koseki et al., 2017). In the enrichment heatmap, numbers shown are odds ratio indicating the possibility of enrichment, with hypergeometric p -value in parenthesis. **B**, RRHO maps comparing ranked logFC of genes from the $\alpha 9k1$ data and the logFC of same genes from DRGs with sciatic nerve injury. The $\alpha 9k1$ -naive group is correlated with the peripherally injured DRGs, especially the downregulated genes on both time points, 1 and 5 d after axotomy (top right corner). Each pixel represents the overlap between genes from two different datasets, color-coded according to the $-\log_{10}$ p -value of a hypergeometric test (step size = 200). On each map, the extent of shared upregulated genes is displayed in the top right corners, whereas shared downregulated genes are displayed in the bottom left corners. **C**, RRHO maps comparing ranked logFC of genes from the $\alpha 9k1$ data and the logFC of same genes from embryonic DRG neurons at E12.5 and E17.5. However, there were no significant correlation between any of the experimental groups, and genes expressed during embryonic axon growth.

shown in the network diagram (Fig. 7A) and the table of mRNAs associated with GO terms (Extended Data Fig. 7-1). Comparison with a previous network of molecules related to axonal transport and trafficking also showed strong correlations, revealing a set of densely networked molecules mostly associated with endosomal transport (Figs. 7C,D, 8A; Koseki et al., 2017). Network analysis revealed that these groups of molecules were highly co-expressed (Fig. 7A). Interestingly, in contrast to the pink and turquoise modules, very few of the genes in the regeneration-related cluster and modules were recognized RAGs (as highlighted in Extended Data Fig. 7-2), apart from the kinase Camk2d, vesicle-related Pcd6ip, autophagy-related Tbc1d14, and ubiquitin-related Usp4 and Lnx1, all of which appear in the Chandran et al., RAGs list. In addition, two casein kinases, CSNK1D and CSNK1A1, were upregulated in the $\alpha 9k1$ -crush condition, which was of interest because association of casein kinases with axon regeneration has been reported previously (Ayad et al., 2016).

←

interaction. **B**, For the pink/turquoise modules, these diagrams show extensive interactions between the inflammation, transcription, signaling, ubiquitin, and localization molecules that were regulated by expression of $\alpha 9$ integrin and kindlin-1, with or without dorsal root crush. **C**, When focusing on transport and trafficking-related molecules in the magenta, black, pink, and turquoise modules, the $\alpha 9k1$ -crush group upregulated the highest degree of transport-related molecules in the four modules which play a crucial role in axon regeneration. **D**, The top 100 most connected or hub genes related to transport. These genes are also enriched in the RAG_Chandran and Transport_Koseki datasets in Figure 8A.

Comparison with gene expression during development

While regeneration shares mechanisms with embryonic development, the molecules involved are often different and expression changes after mammalian spinal cord injury generally do not closely recapitulate development (Harty et al., 2003; Nacu and Tanaka, 2011; Seifert et al., 2019). However, a study of expression changes in cortical neurons regenerating their axons into spinal embryonic grafts found a partial recapitulation of the embryonic gene expression pattern (Poplawski et al., 2020). A recent profiling study of peripheral nerve regeneration has found only minor correlation between the changes after peripheral axotomy and embryonic development (Renthal et al., 2020).

We compared overlap between our modules with embryonic expression in sensory neurons in the database of Tedeschi et al. (2016) using Fisher's exact test (Materials and Methods). The pink module showed modest overlap with embryonic day (E) 17.5 DRG expression in the initial eigengene correlation module analysis (Fig. 8A). We also compared the logFCs of genes in the experimental groups with gene expression in embryonic DRGs at E12.5 and E17.5 (Tedeschi et al., 2016) using the RRHO analysis (Fig. 8C). There was no significant correlation between any of the experimental groups, and genes expressed during embryonic axon growth (logFC E12.5 vs E17.5). Of the ubiquitin-related and autophagy genes upregulated in our regeneration group, there were no or minor changes between adult versus embryonic in the Tedeschi database. Thus, we observed only modest recapitulation of the embryonic expression pattern following $\alpha 9k1$ expression and regeneration after crush injury.

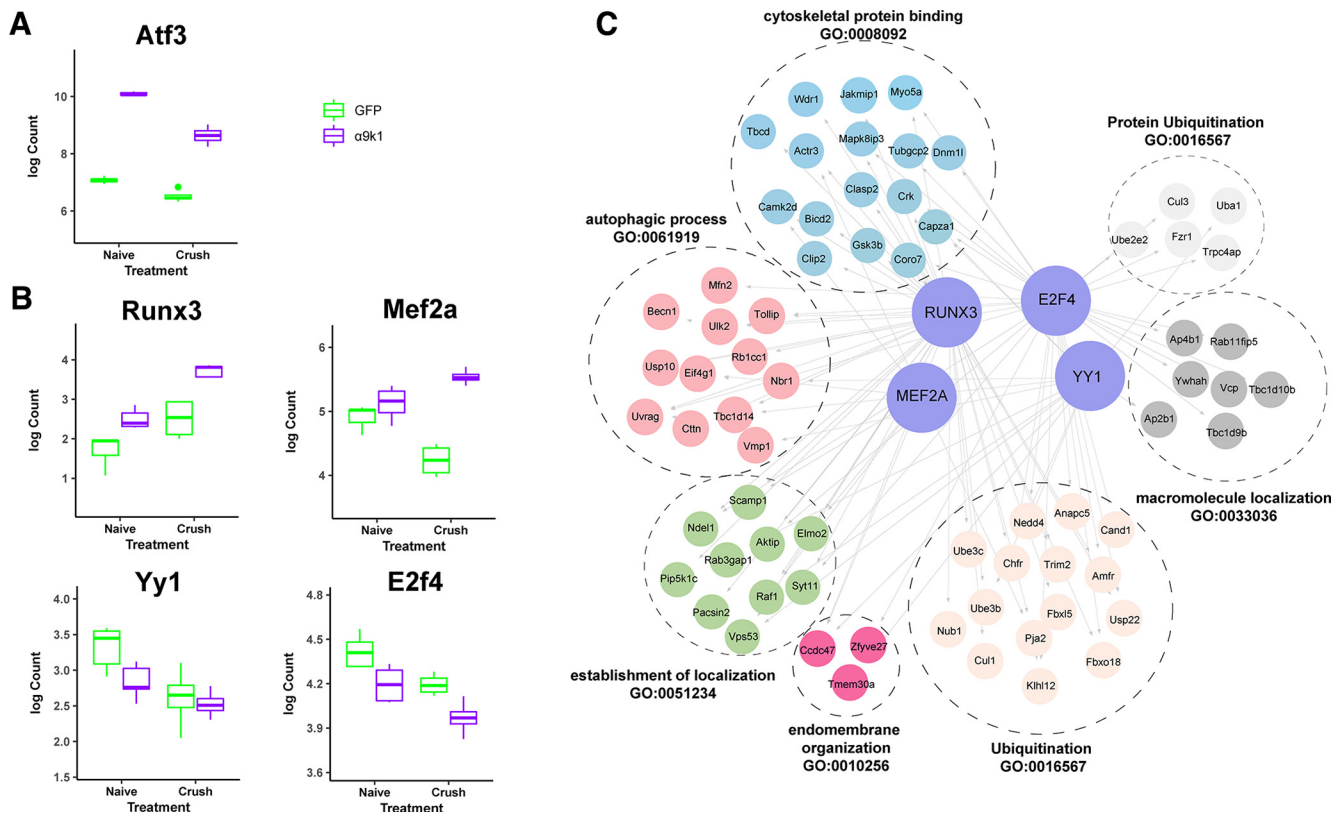


Figure 9. Transcriptional Control of the CNS regeneration program. **A**, Expression levels of a typical RAG, *Atf3*, demonstrating upregulation in both experimental groups in which there were $\alpha 9k1$ overexpression. **B**, Expression levels of four potential transcriptional controllers of the CNS regeneration program: *Runx3*, *Mef2a*, *Yy1*, and *E2f4*. *Runx3* and *Mef2a* are upregulated in the $\alpha 9k1$ -crush (CNS regeneration) groups, while *Yy1* and *E2f4* are downregulated. **C**, TF enrichment analysis of the four potential transcriptional controllers *Runx3*, *Mef2a*, *E2f4*, and *Yy1*. These transcription controllers could regulate the ubiquitination, autophagy and localization processes that are upregulated in Cluster 1 and in the black/magenta modules associated with sensory regeneration.

Transcriptional regulation of the PNS and CNS regeneration programs

To identify potential TF activators and repressors that might regulate the PNS and CNS regeneration programs, we performed a TF enrichment analysis in the promoters of the genes in key regeneration associated modules (Materials and Methods). We aimed to identify TFs that are both present and have regulatory targets in the modules representing the PNS and CNS programs. For the PNS regeneration program there are many potential regulators. Many TFs in the RAGs module from Chandran et al., were regulated by integrin expression and have binding sites in the pink and turquoise modules, including *Jun*, *JunB*, *Egr1*, *Rela*, *Crem*, *Atf2*, *Atf3*, *Fos*, *Cebpd*, *Runx2*, *Stat3*, and *Bhlhe40*. The expression pattern of *Atf3* is shown as an example (Fig. 9A). However, fewer transcription factors were found in the black and magenta modules representing the CNS regeneration program. As potential regulators of ubiquitination, autophagy, ER, localization and cytoskeletal binding genes that appear in the modules associated with the CNS regeneration program we identified *Mef2a*, *Runx3*, *E2f4*, and *Yy1* (Fig. 9B). These molecules have high kME values consistent with hub roles in their modules. TF enrichment analysis predicts many connections between these TFs and the CNS regeneration program targets (Fig. 9C). Expression levels across the experimental groups show that *Runx3* and *Mef2a* are upregulated in the $\alpha 9k1$ -crush condition (CNS regeneration) correlating with their presence in the black and magenta modules, while transcriptional repressor *Yy1* and *E2f4* from the purple module (downregulated in $\alpha 9k1$ -crush) are downregulated (Fig. 9B).

Central sensory nerve regeneration is associated with upregulation of ubiquitin, autophagy, and ER-related mRNAs

A novel finding of this study was the upregulation of many ubiquitin-related molecules in the $\alpha 9k1$ -crush (CNS regeneration) group, seen in Cluster 1 and magenta/black modules (Figs. 5C, 7A; Extended Data Fig. 7-1). Many of these molecules are related to ubiquitination via SCF complexes (SKP, Cullin, F-Box), specifically E3 ubiquitin ligases that attach ubiquitin to molecules via the K48 and K11 lysine residues and associated adaptor/recognition molecules (marked yellow in Extended Data Fig. 7-1; E. Oh et al., 2018a). Based on the analysis, 9 of the upregulated ligases (marked gray in Extended Data Fig. 7-1) ubiquitinate via the K63 position. This form of ubiquitination is commonly associated with modulation of function of enzymes and trafficking of molecules and receptors (E. Oh et al., 2018a).

UbiNet (Nguyen et al., 2016) was used to search for ubiquitination networks and hubs among mRNAs expressed in the magenta/black/turquoise modules as these modules were highly upregulated in the $\alpha 9k1$ -crush (CNS regeneration) group (Materials and Methods). This revealed four main ubiquitination networks (Fig. 10). The cullin family and *Btrc* are the nodes of a network (Fig. 10A) associated with ubiquitination of molecules targeted to the proteasome, including the SCF complex together with SKP1 and F-Box proteins, and interacting E3 ligases. Molecules believed to interact with cullins are outlined in yellow in Extended Data Figures 7-1 and 7-2. A second smaller network has *Nedd4* and *Nedd4L* as hubs (Fig. 10B). These ubiquitin ligases have already been associated with axon growth through

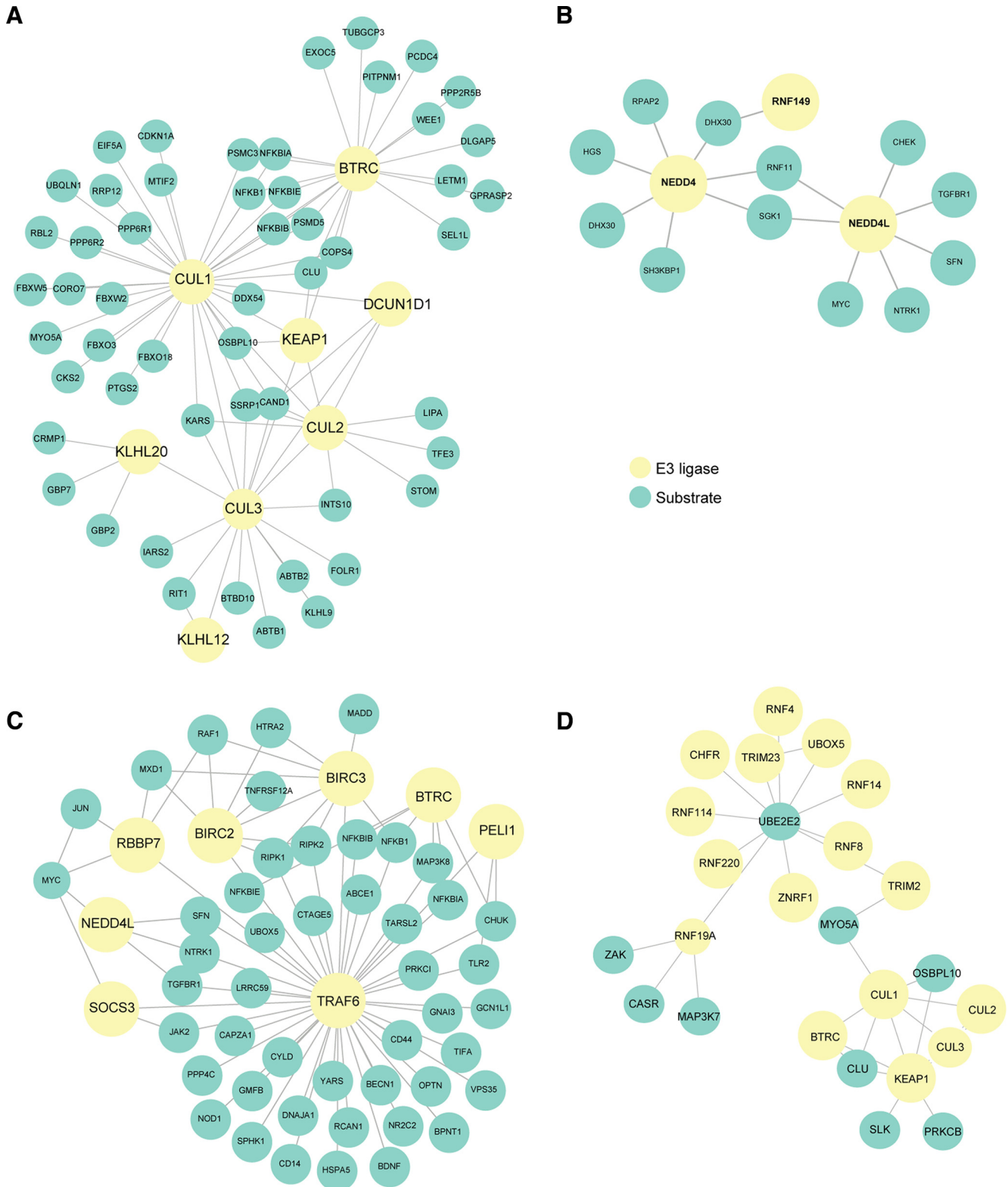


Figure 10. Analysis of ubiquitin-related mRNAs upregulated during sensory regeneration using UbiNet. **A**, An extensive network centers around the cullin family and Btrc, which is associated with ubiquitination of molecules targeted to the proteasome. **B**, A smaller network with Nedd4 and Nedd4L as hubs, which could potentially be associated with regulation of axon growth via interactions with PTEN and mTORC1. **C**, A network centers around the hub Traf6, an E3 ligase implicated in promoting tumorigenesis and invasion through activation of AKT signaling and in control of the NF- κ -B (NFKB) family. **D**, A network with mostly Ube2e2 and Keap1 as hubs which is associated with oxidative stress and neuroprotection.

interactions between PTEN and mTORC1 (Drinjakovic et al., 2010; Christie et al., 2012; Hsia et al., 2014). A further network (Fig. 10C) centers around the hub Traf6, an E3 ligase implicated in promoting tumorigenesis and invasion through activation of

AKT signaling (Yang et al., 2009; Feng et al., 2014) and in control of NF- κ -B. A fourth network (Fig. 10D) is associated with oxidative stress and neuroprotection. It has Ube2e2 and Keap1 as hubs: Ube2e2 is an E2 ubiquitin conjugating enzyme, while

Keap1 is a substrate-specific adaptor that senses oxidative stress acting through the cullin-3 complex (Kobayashi et al., 2004).

Autophagy was a significant term in Cluster 1 and the magenta module. Only three of the Atg genes, which code for autophagosome structural molecules, were upregulated. However, there was upregulation of several transcripts coding molecules that play a key role in the initiation and control of autophagy (Extended Data Fig. 7-1). Optineurin, NBR1 and FIP200 are autophagy receptors that recognize ubiquitin chains; ULK, Beclin, VMP1, PAQR3, and Pik3c3 form a complex that generates local PI(3)P recognized by dfcp1 to initiate autophagosome formation; LC3 and Gabarap are part of the autophagosome membrane; VMP1 is ER-linked and participates in autophagosome formation and VCP in autophagosome maturation (Dikić, 2017; Kulkarni et al., 2018; Kuijpers et al., 2021).

Inhibition of ubiquitination, autophagy, and casein kinases affect *in vitro* axon regeneration

The pattern of expression after $\alpha 9$ k1-crush (CNS regeneration) suggests that increases in ubiquitination and autophagy are involved in central axon regeneration, and two type-1 casein kinases were also upregulated. To test whether these processes are necessary for adult sensory axon regeneration, we applied specific inhibitors to explants of adult rat DRG explants whose axons were allowed to grow for 5 d before axotomy (Fig. 11A–C). We also tested regeneration after axotomy from human iPSC-derived sensory neurons (Singec et al., 2020; Deng et al., 2023) to exclude species differences, that were grown as spot cultures after 21 d of maturation, and whose axons were axotomized with a laser 400–600 μ m away from the cell body (Fig. 11D–F). These assays test regeneration of all axons growing from the cultures, which are presumably a mixture of centrally and peripherally projecting types. Adult sensory neurons *in vitro* develop many processes and do not show a single axon splitting into central and peripheral branches as would be seen *in vivo* and there is currently no method to identify central and peripheral branches. In the rat DRG explants, regeneration of cut axons began after 20 min, and the percentage of regenerating axons was measured at 2 h (Fig. 11A). As a control to exclude nonspecific toxicity and ask whether the effects of the inhibitors were specific to regeneration, continuing growth of uncut axons was also measured (Fig. 11B). This showed that all but one of the inhibitors did not affect continuing outgrowth at the same concentration as they inhibited regeneration. Only the autophagy inhibitor, 3MA, affected both continuing outgrowth and regeneration (Fig. 11B). This inhibitor was tested at various concentrations to show that its threshold concentration for affecting regeneration was the same as that for affecting continuing growth (data not shown). The other inhibitors were not tested at different concentrations so other side effects cannot be excluded. Regeneration of the human iPSC-derived sensory neurons was slower, and regeneration was assayed at 6–24 h (Fig. 11D). In these assays spontaneous regeneration is already maximal in rat DRG explants (70–80% of axons), and as high as 50–70% in human iPSC-derived sensory neurons, so they are useful for testing potential inhibitors of regeneration. In previous studies on rat DRGs, interventions that block regeneration may have little effect on the continuing growth of uncut axons (Chierzi et al., 2005; Verma et al., 2005).

The inhibitors used in these two rat and human *in vitro* assays were used at standard concentrations validated in experiments on neurons in previous papers (examples cited). They were MLN492 (inhibits NEDD8 activating enzyme and blocks ubiquitination associated with the SKP, Cullin, F-box complex; Vogl et

al., 2020); NSC697923 (blocks K63-type ubiquitin ligases by blocking the E2 conjugating enzyme; Cheng et al., 2014); MG132 (proteasome inhibitor; Rousset et al., 2015); 3MA [inhibits class 3 PI3Ks which locate omegasome (autophagosome precursor) production to the surface of the ER; M.V. Rao et al., 2023]; D4476 inhibits Casein Kinase 1 (Nguyen Hoang et al., 2022). In the rat DRG explants, all inhibitors partially blocked regeneration, with the strongest effects from the inhibition of autophagy and E2 conjugating enzyme (Fig. 11A). However, only inhibition of autophagy affected continuing axon growth without axotomy (Fig. 11B). In the human iPSC-derived neurons, inhibitors of autophagy, degradative proteasome, ubiquitination, and casein kinases all inhibited regeneration, but blocking K63-type ubiquitination did not (Fig. 11D). Overall, these experiments show that blocking autophagy, ubiquitination and degradation inhibits the regeneration of injured sensory axons, but only autophagy block affects the continuing growth of uncut/intact axons. The experiments do not address potential differences between central and peripheral sensory axons but suggest that these basic cellular processes may be involved in the regeneration of sensory axons in general.

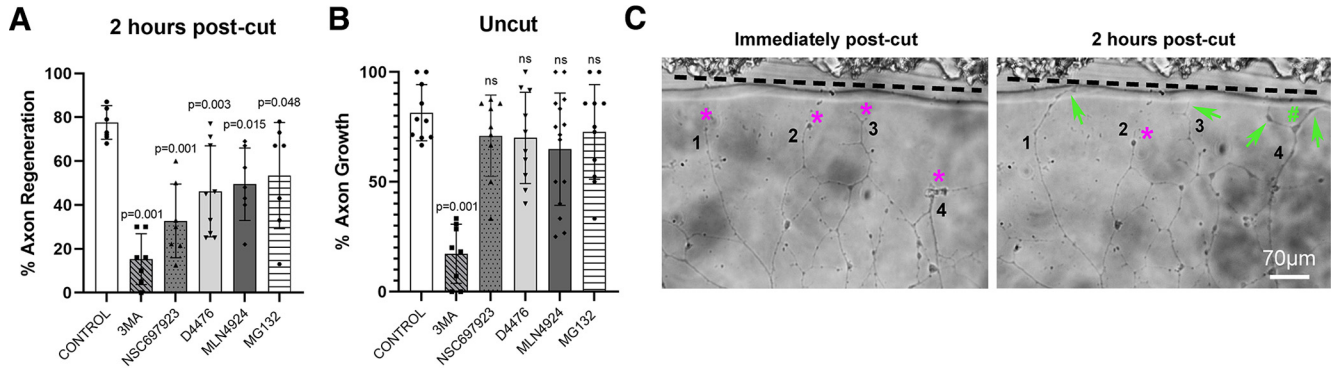
Discussion

The mechanisms by which extrinsic signals influence neuronal programs for regeneration in the CNS are not well understood. Here, we leveraged an adult rat model whereby integrin expression enables long-distance axon regeneration in the CNS central branches of DRG sensory axons, to elucidate the intrinsic growth programs. We were able to deconvolute expression changes caused by integrin expression alone from those caused by integrin-driven regeneration by comparing two groups with very different outcomes: (1) in the $\alpha 9$ k1-naive group integrin signaling occurred, but the intact sensory axons and terminals in the spinal cord showed no sign of enhanced sprouting; (2) in the $\alpha 9$ k1-crush group, there was an extensive axon regeneration along the cord and terminations in the dorsal horn exactly as seen previously (Cheah et al., 2016). We conclude that signaling from activated integrins primes the neurons, putting them in a regeneration-competent state, very similar to that seen in peripheral nerve regeneration after a peripheral axotomy. However, when the $\alpha 9$ k1-primed neurons are axotomized and regenerate their axons through the CNS environment, activation of a second and previously undiscovered program is required, whose purpose is probably to enable the interaction between the axons, the integrins and their environment.

$\alpha 9$ integrin-kindlin-1 expression upregulates the PNS regeneration program

The RAGs program is upregulated as injured peripheral sensory axons regenerate in the PNS (van Kesteren et al., 2011; Chandran et al., 2016; Tedeschi et al., 2016; Rozenbaum et al., 2018). Several of these RAGs participate in regeneration (Fago et al., 2015; Mehta et al., 2016). A surprising finding was that a substantial fraction of the PNS regeneration RAG program was induced by $\alpha 9$ k1 expression alone (Extended Data Fig. 7-2), including most of the RAGs transcription factors. These changes in expression must have been because of signaling both from transduced $\alpha 9$ and DRG-expressed integrins, all activated by kindlin-1. Integrins signal via focal adhesion kinase and integrin-linked kinase to activate the PI3K/Akt, Ras/Erk, Jnk, Rho/Rac pathways and via mechano-transduction through Piezo/Ca⁺⁺, and Hippo/Yap/Taz (Hynes, 2002; Humphries et al., 2019).

Adult rat DRG explants



D Human iPSC-derived sensory neurons

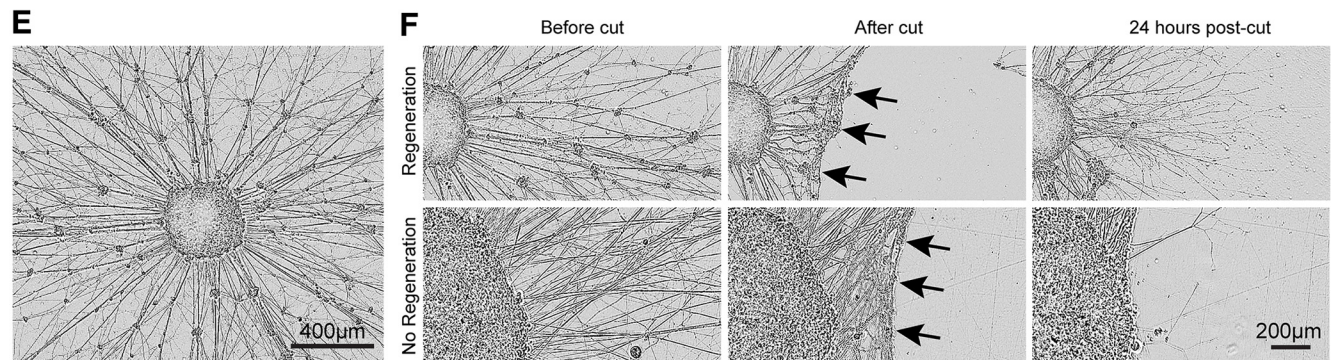
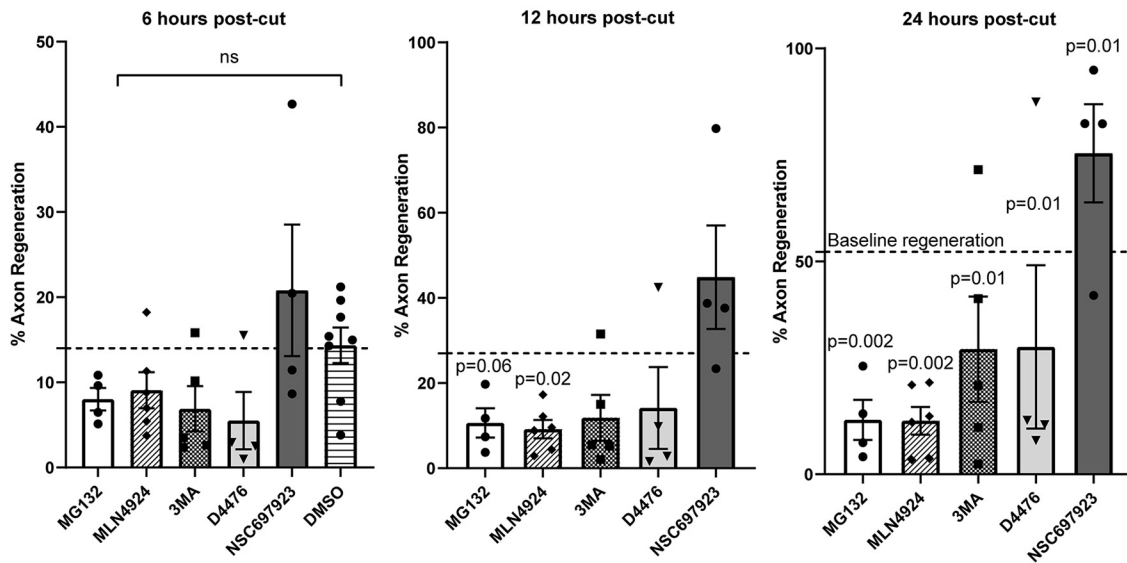


Figure 11. *In vitro* sensory axon regeneration of adult rat DRG explants and human iPSC-derived sensory neurons after axotomy in the presence of inhibitors. The inhibitors used were MLN492, NEDD8-mediated ubiquitination inhibitor; NSC697923, K63-ubiquitination inhibitor; MG132, proteasome inhibitor; 3MA, Class III PI3K autophagy inhibitor; D4476, casein kinase 1 inhibitor. **A, B**, For axotomized axons (**A**) in adult rat DRG explants, all the five inhibitors exhibited various degrees but significant inhibition to axon regeneration, with the greatest effect observed by 3MA and the most modest effect by MG132. For uncut axons (**B**), all inhibitors, except 3MA, did not affect continuous axon growth. Each point represents one experiment involving at least three DRGs with multiple cut axons. Analysis was performed using one-way ANOVA with *post hoc* test. A *p*-value of <0.05 was considered to be statistically significant. **p*-value < 0.05, ***p*-value < 0.01, ****p*-value < 0.001. **C**, Adult rat DRG explant neurites immediately and 2 h after axotomy by a glass-pulled pipette where the demarcation line is shown clearly (black dotted line). Immediately after axotomy, retraction bulbs (magenta asterisks) can be seen for Neurites 1, 2, 3, and 4. Two hours after axotomy, Neurites 1, 3, and 4 regenerated with the formation of growth cones (green arrows), and axon branching (green hash sign) can be seen for Neurite 4. **D**, The percentage of human iPSC-derived sensory axons regenerating at 6, 12, and 24 h after laser axotomy, and regeneration was inhibited by all the inhibitors except NSC697923. Analysis was performed using Fisher's exact test. The *p*-values were then analyzed with the "Analyze a stack of *p*-values" function in GraphPad Prism with a Bonferroni–Dunn pairwise comparison. **E**, An aggregate of human iPSC-derived sensory neurons with halo of axons, after 21 d of maturation. **F**, The results of laser axotomy of the halo of axons. After axotomy, the axons retracted (black arrows) followed by various degrees of regeneration in the presence of inhibitors in the post-24 h.

Many of the RAG genes and DRG integrins have been linked to regeneration in peripheral nerves (Werner et al., 2000a,b; Voglezang et al., 2001; Liu et al., 2009; Patodia and Raivich, 2012; Fagoe et al., 2014; Ma and Willis, 2015; Nieuwenhuis et al., 2018). Expression of $\alpha 9k1$ in sensory neurons will therefore enhance regeneration in peripheral nerves.

$\alpha 9$ integrin-kindlin-1-driven regeneration upregulates a CNS regeneration group of genes

By comparing the $\alpha 9k1$ dorsal root crush and naive groups, we were able to identify genes that were specifically associated with central axon regeneration in the spinal cord, present as Cluster 1 in the heatmap (Figs. 4, 5C) and in the magenta/black modules (Fig. 7A). In these regeneration-associated cluster and modules, the most significant GO terms were related to transport/trafficking, ubiquitination, autophagy, endoplasmic reticulum, endomembrane organization, signaling and cytoskeletal binding (Figs. 5C, 7A; Extended Data Fig. 7-1). These processes are presumably involved in bringing molecules to growth cones and recycling them to enable axon growth through the CNS environment.

Transport and trafficking

Transport and trafficking upregulation in axon regeneration have been recognized for many years (Grafstein and Murray, 1969; Oblinger et al., 1987). The molecules needed to build growing axons come partly from the cell body via axonal transport, and partly from local translation within axons (Koley et al., 2019; Smith et al., 2020). In our CNS regeneration gene group, transcripts upregulated were associated with molecular motors, endocytosis, exocytosis, vesicle sorting, scaffolding, ArfGAPs, Golgi and ER. Two scaffolding molecules, Ywhaz (14.3.3 protein) and Zfyve27 (Protrudin), are of particular interest because both are associated with the promotion of CNS axon regeneration, and Protrudin achieves this by linking trafficking to the ER (Kaplan et al., 2017; Petrova et al., 2020).

Ubiquitination

Several individual ubiquitin ligases have been implicated in control of axon growth through removal of growth-control molecules (Hsia et al., 2014; Y.M. Oh et al., 2018b; Sakai et al., 2021). Ubiquitination molecules of several types were present in the regeneration-associated Cluster 1 (Fig. 5C) and magenta/black modules (Fig. 7A). Many were related to the degradative ubiquitination-proteasome pathway in which E3 ligases associate with the SCF complexes (SKP, Cullin, F-Box), attaching ubiquitin to molecules via the K48 and K11 lysine residues of ubiquitin (Zinngrebe et al., 2014; Dikic, 2017; E. Oh et al., 2018a). Within this group there were cullins, E3 ligases and adaptors. K63 ubiquitination does not usually lead to degradation, but can modulate the function of signaling and transport molecules and marks molecules for trafficking and recycling (E. Oh et al., 2018a); there were several E3 ligases of this type. We used UbiNet to search for potential ubiquitination networks (Nguyen et al., 2016), identifying four networks with hubs (Fig. 10). (1) Cullins are the key component of the SCF box complex, and molecules ubiquitinated by this mechanism are usually targeted for proteasomal degradation (Fig. 10A; E. Oh et al., 2018a). In combination with the substrate adaptor KLH20, cullin-3 has been implicated in neurotrophin-induced axon growth through degradation of RhoGEF (Lin et al., 2011). (2) Nedd4 and Nedd4L hubs (Fig. 10B). Nedd4 has been implicated in axon growth, although the

mechanism is disputed between targeting PTEN for degradation, or as a target of PTEN and mTORC1 (Drinjakovic et al., 2010; Hsia et al., 2014). (3) E3 ligase Traf6 (Fig. 10C) controls NF- κ -B levels, Jun and PI3Kinase-AKT signaling (Hamidi et al., 2017), and also controls autophagy (Nazio et al., 2013). (4) Keap1 and the E2 ligase Ube2e2 (Fig. 10D) acts as an oxidative stress sensor (Kobayashi et al., 2004), potentially providing neuroprotection.

In addition to the upregulated mRNAs discussed above, significant inhibitors of regeneration were downregulated after axotomy and $\alpha 9k1$. These were Wnt and Notch mRNAs and their receptors Frizzled, Ryk, and Jagged.

Autophagy

Autophagy control molecules were also present in the $\alpha 9k1$ -crush (regeneration) group. These include ULK1, and Pik3c3 and Beclin-1, controllers of autophagosome production (Maday and Holzbaur, 2016; Winckler et al., 2018; Ktistakis, 2020). Selective autophagy links the ER, recycling endosomes and ubiquitination, all implicated in axon regeneration (Eva et al., 2012; Petrova et al., 2020), and ubiquitinated molecules are recognized by autophagy recognition molecules such as NBR1, FIP200 and optineurin (present in our magenta and black modules; Fig. 7A; Hara et al., 2008; Kenific and Debnath, 2016; Mowers et al., 2017). Autophagy can act as a recycling pathway for integrins and focal adhesions in cell migration (Abbi et al., 2002; Tuloup-Minguez et al., 2013; Kenific and Debnath, 2016; Kenific et al., 2016; Maday and Holzbaur, 2016; Sharifi et al., 2016; Wei et al., 2017). This pattern of ubiquitin molecule expression in the CNS regeneration program is not seen in PNS regeneration studies (Chandran et al., 2016; Tedeschi et al., 2016). Autophagy has previously been linked to axon growth through cytoskeletal stabilization and growth cone motility (He et al., 2016; Sakamoto et al., 2019; Ko et al., 2020).

Endoplasmic reticulum

Endoplasmic reticulum-related genes were also upregulated. The presence of endoplasmic reticulum in axon growth cones is a requirement for successful regeneration (Raiborg et al., 2015; K. Rao et al., 2016; Petrova et al., 2020). Endoplasmic reticulum is a source of autophagosomes, generation being controlled by ULKs, Beclin and PIK3C (Dikic, 2017; Stavoe and Holzbaur, 2018), which were upregulated in our regeneration group.

Validation of involvement in axon regeneration

To confirm that the K48 and K63 ubiquitination pathway and autophagy are involved in axon regeneration, we tested inhibitors on regeneration of axotomized adult rat DRG axons and human iPSC-derived sensory neurons *in vitro*. All the inhibitors reduced axon regeneration of rat sensory axons. However, only the autophagy inhibitor affected continuing growth of uncut axons, confirming that regeneration of a new growth cone requires specific mechanisms that are not necessary for continuing growth (Bradke et al., 2012). These experiments demonstrate an effect of acute administration of the inhibitors on sensory axon regeneration. However, they do not distinguish between regeneration of the peripheral and central branches of the sensory axons. Currently this is not practicable, because there is no label to distinguish central and peripheral axons *in vitro*, we assume that half the axons will be of central branch type, but this is unproven. It is also not practicable to ask whether inhibition of autophagy, ubiquitination, protein degradation *in vivo* during the prolonged time needed for sensory regeneration, because blocking these essential biological functions leads to accumulation of organelles and damaged proteins, leading to a

neurodegenerative condition (Komatsu et al., 2006; Lehman, 2009; Mallucci et al., 2020) which will confound attempts to measure effects on regeneration. The finding in this study is that the mRNAs for these processes are upregulated during CNS regeneration indicating that growth through CNS tissue requires additional involvement of autophagy, ubiquitination, and degradation. However, these are basic cellular processes and therefore reducing them below normal levels will likely affect many cellular functions.

Control of the PNS and CNS regeneration programs

The current study shows that signaling from activated integrins alone is sufficient to upregulate many transcripts of the RAGs program. For control of the CNS regeneration program, we identified *Mef2a*, *Runx3*, *E2f4*, and *Yy1* as potential regulators of autophagy, trafficking, ubiquitination and ER. *Runx3* is involved in sensory axon guidance and connectivity, *Mef2a* acts via p38 which has many functions in axon growth, *Yy1* has a role in hippocampal axon growth and control of autophagy, and *E2F4* has a role in spinal axon regeneration and autophagy (de Angelis et al., 2005; Chen et al., 2006; Lallemand et al., 2012; Klar et al., 2015; Qiang et al., 2016; Du et al., 2019).

$\alpha 9$ integrin-kindlin-1-driven axon regeneration does not recapitulate embryonic development

The issue of whether integrin-kindlin-driven regeneration represents a return to an embryonic pattern of expression is of obvious interest. In general, repair does not accurately recapitulate development (Harty et al., 2003; Nacu and Tanaka, 2011; Seifert et al., 2019), although basic mechanisms of cell movement are shared. In previous studies, embryonic recapitulation was marginally significant in peripheral nerve regeneration (Renthal et al., 2020). In cortical neurons elongating into embryonic grafts there was significant embryonic recapitulation (Poplawski et al., 2020). In our study comparisons between the $\alpha 9$ k1 regeneration group and a previous study of sensory neuron expression at E12.5 and E17.5 (Tedeschi et al., 2016) showed no correlation.

Overall, the study suggests that axon regeneration in the CNS comprises two steps. In the first priming step, various transcripts, including those identified as RAGs, are upregulated by signaling from $\alpha 9$ k1. As a second step there is a set of transcripts involved in enabling axon growth through the CNS environment, which we found to be only upregulated in the $\alpha 9$ k1 crush/CNS regeneration group. These are involved in transport/trafficking, ubiquitination, autophagy, endoplasmic reticulum, endomembrane organization, cytoskeletal binding, and probably enable the transport and trafficking of regeneration-associated molecules and organelles, interaction with the CNS environment, and signaling. Expression of $\alpha 9$ k1 therefore enables regeneration in three ways. It provides an appropriate adhesion receptor to drive migration of axon growth cones, it activates the genetic program associated with regeneration in peripheral nerves (the RAGs program) and it enables expression of a third set of genes upregulated by axotomy and regeneration, which presumably permit axons to grow in the adult CNS environment.

References

- Abbi S, Ueda H, Zheng C, Cooper LA, Zhao J, Christopher R, Guan JL (2002) Regulation of focal adhesion kinase by a novel protein inhibitor FIP200. *Mol Biol Cell* 13:3178–3191.
- Andrews MR, Czvitkovich S, Dassi E, Vogelaar CF, Faissner A, Blits B, Gage FH, Ffrench-Constant C, Fawcett JW (2009) Alpha9 integrin promotes neurite outgrowth on tenascin-C and enhances sensory axon regeneration. *J Neurosci* 29:5546–5557.
- Ayad NG, Lee JK, Lemmon VP (2016) Casein kinase signaling in axon regeneration. *Neural Regen Res* 11:210–211.
- Bradke F, Fawcett JW, Spira ME (2012) Assembly of a new growth cone after axotomy: the precursor to axon regeneration. *Nat Rev Neurosci* 13:183–193.
- Chandran V, et al. (2016) A systems-level analysis of the peripheral nerve intrinsic axonal growth program. *Neuron* 89:956–970.
- Cheah M, Andrews MR, Chew DJ, Moloney EB, Verhaagen J, Fässler R, Fawcett JW (2016) Expression of an activated integrin promotes long-distance sensory axon regeneration in the spinal cord. *J Neurosci* 36:7283–7297.
- Cheah M, Fawcett JW, Andrews MR (2017) Dorsal root ganglion injection and dorsal root crush injury as a model for sensory axon regeneration. *J Vis Exp* (123):55535.
- Chen AI, de Nooij JC, Jessell TM (2006) Graded activity of transcription factor *Runx3* specifies the laminar termination pattern of sensory axons in the developing spinal cord. *Neuron* 49:395–408.
- Chen EY, Tan CM, Kou Y, Duan Q, Wang Z, Meirelles GV, Clark NR, Ma'ayan A (2013) Enrichr: interactive and collaborative HTML5 gene list enrichment analysis tool. *BMC Bioinformatics* 14:128.
- Cheng J, Fan YH, Xu X, Zhang H, Dou J, Tang Y, Zhong X, Rojas Y, Yu Y, Zhao Y, Vasudevan SA, Zhang H, Nuchtern JG, Kim ES, Chen X, Lu F, Yang J (2014) A small-molecule inhibitor of UBE2N induces neuroblastoma cell death via activation of p53 and JNK pathways. *Cell Death Dis* 5:e1079.
- Chierzi S, Ratto GM, Verma P, Fawcett JW (2005) The ability of axons to regenerate their growth cones depends on axonal type and age, and is regulated by calcium, cAMP and ERK. *Eur J Neurosci* 21:2051–2062.
- Christie KJ, Martinez JA, Zochodne DW (2012) Disruption of E3 ligase NEDD4 in peripheral neurons interrupts axon outgrowth: linkage to PTEN. *Mol Cell Neurosci* 50:179–192.
- Curcio M, Bradke F (2018) Axon regeneration in the central nervous system: facing the challenges from the inside. *Annu Rev Cell Dev Biol* 34:495–521.
- de Angelis L, Zhao J, Andreucci JJ, Olson EN, Cossu G, McDermott JC (2005) Regulation of vertebrate myotome development by the p38 MAP kinase-MEF2 signaling pathway. *Dev Biol* 283:171–179.
- Deng T, et al. (2023) Scalable generation of sensory neurons from human pluripotent stem cells. *Stem Cell Reports* 18:1030–1047.
- Dikic I (2017) Proteasomal and autophagic degradation systems. *Annu Rev Biochem* 86:193–224.
- Dobbertin A, Czvitkovich S, Theodoridis U, Garwood J, Andrews MR, Properzi F, Lin R, Fawcett JW, Faissner A (2010) Analysis of combinatorial variability reveals selective accumulation of the fibronectin type III domains B and D of tenascin-C in injured brain. *Exp Neurol* 225:60–73.
- Dobin A, Davis CA, Schlesinger F, Drenkow J, Zaleski C, Jha S, Batut P, Chaisson M, Gingeras TR (2013) STAR: ultrafast universal RNA-seq aligner. *Bioinformatics* 29:15–21.
- Drinjakovic J, Jung H, Campbell DS, Strohlic L, Dwivedy A, Holt CE (2010) E3 ligase Nedd4 promotes axon branching by downregulating PTEN. *Neuron* 65:341–357.
- Du J, Ren W, Yao F, Wang H, Zhang K, Luo M, Shang Y, O'Connell D, Bei Z, Wang H, Xiong R, Yang Y (2019) YY1 cooperates with TFEB to regulate autophagy and lysosomal biogenesis in melanoma. *Mol Carcinog* 58:2149–2160.
- El Bejjani R, Hammarlund M (2012) Notch signaling inhibits axon regeneration. *Neuron* 73:268–278.
- Eva R, Crisp S, Marland JR, Norman JC, Kanamarlapudi V, Ffrench-Constant C, Fawcett JW (2012) ARF6 directs axon transport and traffic of integrins and regulates axon growth in adult DRG neurons. *J Neurosci* 32:10352–10364.
- Fagoie ND, van Heest J, Verhaagen J (2014) Spinal cord injury and the neuron-intrinsic regeneration-associated gene program. *Neuromolecular Med* 16:799–813.
- Fagoie ND, Attwell CL, Kouwenhoven D, Verhaagen J, Mason MR (2015) Overexpression of ATF3 or the combination of ATF3, c-Jun, STAT3 and Smad1 promotes regeneration of the central axon branch of sensory neurons but without synergistic effects. *Hum Mol Genet* 24:6788–6800.
- Feng H, et al. (2014) EGFR phosphorylation of DCBLD2 recruits TRAF6 and stimulates AKT-promoted tumorigenesis. *J Clin Invest* 124:3741–3756.

- Golan N, Kauer S, Ehrlich DB, Ravindra N, van Dijk D, Cafferty WB (2021) Single-cell transcriptional profiling of the adult corticospinal tract reveals forelimb and hindlimb molecular specialization. *bioRxiv* 446653.
- Grafstein B, Murray M (1969) Transport of protein in goldfish optic nerve during regeneration. *Exp Neurol* 25:494–508.
- Hamidi A, Song J, Thakur N, Itoh S, Marcusson A, Bergh A, Heldin CH, Landström M (2017) TGF- β promotes PI3K-AKT signaling and prostate cancer cell migration through the TRAF6-mediated ubiquitylation of p85 α . *Sci Signal* 10:eaal4186.
- Hansen KD, Irizarry RA, Wu Z (2012) Removing technical variability in RNA-seq data using conditional quantile normalization. *Biostatistics* 13:204–216.
- Hara T, Takamura A, Kishi C, Iemura S, Natsume T, Guan JL, Mizushima N (2008) FIP200, a ULK-interacting protein, is required for autophagosome formation in mammalian cells. *J Cell Biol* 181:497–510.
- Harty M, Neff AW, King MW, Mescher AL (2003) Regeneration or scarring: an immunologic perspective. *Dev Dyn* 226:268–279.
- He M, Ding Y, Chu C, Tang J, Xiao Q, Luo ZG (2016) Autophagy induction stabilizes microtubules and promotes axon regeneration after spinal cord injury. *Proc Natl Acad Sci U S A* 113:11324–11329.
- Ho TS-Y, Hees JT, Xu Z, Kawaguchi R, Biscola NP, Taub DG, Chen K, Chen X, Barrett LB, Cheng L, Gabel CV, Havton LA, Geschwind DH, Woolf CJ (2021) Screening for axon regeneration promoting compounds with human iPSC-derived motor neurons. *bioRxiv* 466937.
- Hsia HE, Kumar R, Luca R, Takeda M, Courchet J, Nakashima J, Wu S, Goebbels S, An W, Eickholt BJ, Polleux F, Rotin D, Wu H, Rossner MJ, Bagni C, Rhee JS, Brose N, Kawabe H (2014) Ubiquitin E3 ligase Nedd4-1 acts as a downstream target of PI3K/PTEN-mTORC1 signaling to promote neurite growth. *Proc Natl Acad Sci U S A* 111:13205–13210.
- Humphries JD, Chastney MR, Askari JA, Humphries MJ (2019) Signal transduction via integrin adhesion complexes. *Curr Opin Cell Biol* 56:14–21.
- Hynes RO (2002) Integrins: bidirectional, allosteric signaling machines. *Cell* 110:673–687.
- Kaplan A, Morquette B, Kroner A, Leong S, Madwar C, Sanz R, Banerjee SL, Antel J, Bisson N, David S, Fournier AE (2017) Small-molecule stabilization of 14-3-3 protein-protein interactions stimulates axon regeneration. *Neuron* 93:1082–1093.e5.
- Kenific CM, Debnath J (2016) NBR1-dependent selective autophagy is required for efficient cell-matrix adhesion site disassembly. *Autophagy* 12:1958–1959.
- Kenific CM, Wittmann T, Debnath J (2016) Autophagy in adhesion and migration. *J Cell Sci* 129:3685–3693.
- Klar M, Fenske P, Vega FR, Dame C, Bräuer AU (2015) Transcription factor Yin-Yang 2 alters neuronal outgrowth in vitro. *Cell Tissue Res* 362:453–460.
- Ko SH, Apple EC, Liu Z, Chen L (2020) Age-dependent autophagy induction after injury promotes axon regeneration by limiting NOTCH. *Autophagy* 16:2052–2068.
- Kobayashi A, Kang MI, Okawa H, Ohtsuiji M, Zenke Y, Chiba T, Igarashi K, Yamamoto M (2004) Oxidative stress sensor Keap1 functions as an adaptor for Cul3-based E3 ligase to regulate proteasomal degradation of Nrf2. *Mol Cell Biol* 24:7130–7139.
- Koley S, Rozenbaum M, Fainzilber M, Terenzio M (2019) Translating regeneration: local protein synthesis in the neuronal injury response. *Neurosci Res* 139:26–36.
- Komatsu M, Waguri S, Chiba T, Murata S, Iwata JI, Tanida I, Ueno T, Koike M, Uchiyama Y, Kominami E, Tanaka K (2006) Loss of autophagy in the central nervous system causes neurodegeneration in mice. *Nature* 441:880–884.
- Koseki H, Donegá M, Lam BY, Petrova V, van Erp S, Yeo GS, Kwok JC, Ffrench-Constant C, Eva R, Fawcett JW (2017) Selective rab11 transport and the intrinsic regenerative ability of CNS axons. *Elife* 6:e26956.
- Ktistakis NT (2020) ER platforms mediating autophagosome generation. *Biochim Biophys Acta Mol Cell Biol Lipids* 1865:158433.
- Kuijpers M, Azarnia Tehran D, Haucke V, Soykan T (2021) The axonal endolysosomal and autophagic systems. *J Neurochem* 158:589–602.
- Kuleshov MV, Jones MR, Rouillard AD, Fernandez NF, Duan Q, Wang Z, Koplev S, Jenkins SL, Jagodnik KM, Lachmann A, McDermott MG, Monteiro CD, Gunderson GW, Ma'ayan A (2016) Enrichr: a comprehensive gene set enrichment analysis web server 2016 update. *Nucleic Acids Res* 44:W90–W97.
- Kulkarni A, Chen J, Maday S (2018) Neuronal autophagy and intercellular regulation of homeostasis in the brain. *Curr Opin Neurobiol* 51:29–36.
- Lachmann A, Xu H, Krishnan J, Berger SI, Mazloom AR, Ma'ayan A (2010) ChEA: transcription factor regulation inferred from integrating genome-wide ChIP-X experiments. *Bioinformatics* 26:2438–2444.
- Lallemend F, Sterzenbach U, Hadjab-Lallemend S, Aquino JB, Castelo-Branco G, Sinha I, Villaescusa JC, Levanon D, Wang Y, Franck MC, Kharchenko O, Adameyko I, Linnarsson S, Groner Y, Turner E, Ernfor P (2012) Positional differences of axon growth rates between sensory neurons encoded by Runx3. *EMBO J* 31:3718–3729.
- Langfelder P, Horvath S (2008) WGCNA: an R package for weighted correlation network analysis. *BMC Bioinformatics* 9:559.
- Langfelder P, Zhang B, Horvath S (2008) Defining clusters from a hierarchical cluster tree: the Dynamic Tree Cut package for R. *Bioinformatics* 24:719–720.
- Lehman NL (2009) The ubiquitin proteasome system in neuropathology. *Acta Neuropathol* 118:329–347.
- Lin MY, Lin YM, Kao TC, Chuang HH, Chen RH (2011) PDZ-RhoGEF ubiquitination by Cullin3-KLHL20 controls neurotrophin-induced neurite outgrowth. *J Cell Biol* 193:985–994.
- Liu WQ, Martinez JA, Durand J, Wildering W, Zochodne DW (2009) RGD-mediated adhesive interactions are important for peripheral axon outgrowth in vivo. *Neurobiol Dis* 34:11–22.
- Ma TC, Willis DE (2015) What makes a RAG regeneration associated? *Front Mol Neurosci* 8:43.
- Maday S, Holzbaur EL (2016) Compartment-specific regulation of autophagy in primary neurons. *J Neurosci* 36:5933–5945.
- Mallucci GR, Klenerman D, Rubinsztein DC (2020) Developing therapies for neurodegenerative disorders: insights from protein aggregation and cellular stress responses. *Annu Rev Cell Dev Biol* 36:165–189.
- Mehta ST, Luo X, Park KK, Bixby JL, Lemmon VP (2016) Hyperactivated Stat3 boosts axon regeneration in the CNS. *Exp Neurol* 280:115–120.
- Mowers EE, Sharifi MN, Macleod KF (2017) Autophagy in cancer metastasis. *Oncogene* 36:1619–1630.
- Nacu E, Tanaka EM (2011) Limb regeneration: a new development? *Annu Rev Cell Dev Biol* 27:409–440.
- Nazio F, Strappazzon F, Antoniole M, Bielli P, Cianfanelli V, Bordi M, Gretzmeier C, Dengjel J, Piacentini M, Fimia GM, Cecconi F (2013) mTOR inhibits autophagy by controlling ULK1 ubiquitylation, self-association and function through AMBRA1 and TRAF6. *Nat Cell Biol* 15:406–416.
- Neumann S, Woolf CJ (1999) Regeneration of dorsal column fibers into and beyond the lesion site following adult spinal cord injury. *Neuron* 23:83–91.
- Nguyen VN, Huang KY, Weng JT, Lai KR, Lee TY (2016) UbiNet: an online resource for exploring the functional associations and regulatory networks of protein ubiquitylation. *Database (Oxford)* 2016:baw054.
- Nguyen Hoang AT, Lee H, Lee SJ (2022) Casein kinase I inhibitor D4476 influences autophagy and apoptosis in chloroquine-induced adult retinal pigment epithelial-19 cells. *Exp Eye Res* 218:109004.
- Nieuwenhuis B, Haenzi B, Andrews MR, Verhaagen J, Fawcett JW (2018) Integrins promote axonal regeneration after injury of the nervous system. *Biol Rev Camb Philos Soc* 93:1339–1362.
- Oblinger MM, Brady ST, McQuarrie IG, Lasek RJ (1987) Cytotypic differences in the protein composition of the axonally transported cytoskeleton in mammalian neurons. *J Neurosci* 7:453–462.
- Oh E, Akopian D, Rape M (2018a) Principles of ubiquitin-dependent signaling. *Annu Rev Cell Dev Biol* 34:137–162.
- Oh YM, Mahar M, Ewan EE, Leahy KM, Zhao G, Cavalli V (2018b) Epigenetic regulator UHRF1 inactivates REST and growth suppressor gene expression via DNA methylation to promote axon regeneration. *Proc Natl Acad Sci U S A* 115:E12417–E12426.
- Onishi K, Hollis E, Zou Y (2014) Axon guidance and injury-lessons from Wnts and Wnt signaling. *Curr Opin Neurobiol* 27:232–240.
- Palmisano I, et al. (2019) Epigenomic signatures underpin the axonal regenerative ability of dorsal root ganglia sensory neurons. *Nat Neurosci* 22:1913–1924.
- Patodia S, Raivich G (2012) Role of transcription factors in peripheral nerve regeneration. *Front Mol Neurosci* 5:8.
- Patro R, Duggal G, Love MI, Irizarry RA, Kingsford C (2017) Salmon provides fast and bias-aware quantification of transcript expression. *Nat Methods* 14:417–419.

- Petrova V, Pearson CS, Ching J, Tribble JR, Solano AG, Yang Y, Love FM, Watt RJ, Osborne A, Reid E, Williams PA, Martin KR, Geller HM, Eva R, Fawcett JW (2020) Protrudin functions from the endoplasmic reticulum to support axon regeneration in the adult CNS. *Nat Commun* 11:5614.
- Plaisier SB, Taschereau R, Wong JA, Graeber TG (2010) Rank-rank hypergeometric overlap: identification of statistically significant overlap between gene-expression signatures. *Nucleic Acids Res* 38:e169.
- Poplawski GHD, Kawaguchi R, Van Niekerk E, Lu P, Mehta N, Canete P, Lie R, Dragatsis I, Meves JM, Zheng B, Coppola G, Tuszynski MH (2020) Injured adult neurons regress to an embryonic transcriptional growth state. *Nature* 581:77–82.
- Qiang L, Zhao B, Shah P, Sample A, Yang S, He YY (2016) Autophagy positively regulates DNA damage recognition by nucleotide excision repair. *Autophagy* 12:357–368.
- Raiborg C, Wenzel EM, Pedersen NM, Olsvik H, Schink KO, Schultz SW, Vietri M, Nisi V, Bucci C, Brech A, Johansen T, Stenmark H (2015) Repeated ER-endosome contacts promote endosome translocation and neurite outgrowth. *Nature* 520:234–238.
- Rao K, Stone MC, Weiner AT, Gheres KW, Zhou C, Deitcher DL, Levitan ES, Rolls MM (2016) Spastin, atlastin, and ER relocalization are involved in axon but not dendrite regeneration. *Mol Biol Cell* 27:3245–3256.
- Rao MV, Darji S, Stavrides PH, Goulbourne CN, Kumar A, Yang DS, Yoo L, Peddy J, Lee JH, Yuan A, Nixon RA (2023) Autophagy is a novel pathway for neurofilament protein degradation in vivo. *Autophagy* 19:1277–1292.
- Rauch U (2004) Extracellular matrix components associated with remodeling processes in brain. *Cell Mol Life Sci* 61:2031–2045.
- Reimand J, Arak T, Adler P, Kolberg L, Reisberg S, Peterson H, Vilo J (2016) g: profiler—a web server for functional interpretation of gene lists (2016 update). *Nucleic Acids Res* 44:W83–W89.
- Renthal W, Tochitsky I, Yang L, Cheng YC, Li E, Kawaguchi R, Geschwind DH, Woolf CJ (2020) Transcriptional reprogramming of distinct peripheral sensory neuron subtypes after axonal injury. *Neuron* 108:128–144.e9.
- Ritchie ME, Phipson B, Wu D, Hu Y, Law CW, Shi W, Smyth GK (2015) limma powers differential expression analyses for RNA-sequencing and microarray studies. *Nucleic Acids Res* 43:e47.
- Rosenbloom KR, et al. (2012) ENCODE whole-genome data in the UCSC Genome Browser: update 2012. *Nucleic Acids Res* 40:D912–D917.
- Rousset M, Cens T, Menard C, Bowerman M, Bellis M, Brusés J, Raoul C, Scamps F, Charnet P (2015) Regulation of neuronal high-voltage activated Ca(V)₂ Ca(2+) channels by the small GTPase RhoA. *Neuropharmacology* 97:201–209.
- Rozenbaum M, Rajman M, Rishal I, Koppel I, Koley S, Medzihradsky KF, Osés-Prieto JA, Kawaguchi R, Amieux PS, Burlingame AL, Coppola G, Fainzilber M (2018) Translatome regulation in neuronal injury and axon regrowth. *eNeuro* 5:ENEURO.0276-17.2018.
- Sakai Y, Hanafusa H, Shimizu T, Pastuhov SI, Hisamoto N, Matsumoto K (2021) BRCA1-BARD1 regulates axon regeneration in concert with the Gqα-DAG signaling network. *J Neurosci* 41:2842–2853.
- Sakamoto K, Ozaki T, Ko YC, Tsai CF, Gong Y, Morozumi M, Ishikawa Y, Uchimura K, Nadanaka S, Kitagawa H, Zulueta MML, Bandaru A, Tamura JJ, Hung SC, Kadomatsu K (2019) Glycan sulfation patterns define autophagy flux at axon tip via PTPRσ-cortactin axis. *Nat Chem Biol* 15:699–709.
- Seifert AW, Cook AB, Shaw D (2019) Inhibiting fibroblast aggregation in skin wounds unlocks developmental pathway to regeneration. *Dev Biol* 455:60–72.
- Sharifi MN, Mowers EE, Drake LE, Collier C, Chen H, Zamora M, Mui S, Macleod KF (2016) Autophagy promotes focal adhesion disassembly and cell motility of metastatic tumor cells through the direct interaction of paxillin with LC3. *Cell Rep* 15:1660–1672.
- Singec I, Deng T, Simeonov A (2020) WO/2020/219811 - Nociceptor differentiation from human pluripotent stem cells. Available at https://patentscope.wipo.int/search/en/detail.jsf?docId=WO2020219811&_cid=P21-KUMWLF-29547-1.
- Smith TP, Sahoo PK, Kar AN, Twiss JL (2020) Intra-axonal mechanisms driving axon regeneration. *Brain Res* 1740:146864.
- Stavoe AKH, Holzbaue ELF (2018) Axonal autophagy: mini-review for autophagy in the CNS. *Neurosci Lett* 697:17–23.
- Tedeschi A, Dupraz S, Laskowski CJ, Xue J, Ulas T, Beyer M, Schultze JL, Bradke F (2016) The calcium channel subunit alpha2delta2 suppresses axon regeneration in the adult CNS. *Neuron* 92:419–434.
- Tuloup-Minguez V, Hamai A, Greffard A, Nicolas V, Codogno P, Botti J (2013) Autophagy modulates cell migration and β1 integrin membrane recycling. *Cell Cycle* 12:3317–3328.
- van Kesteren RE, Mason MR, MacGillavry HD, Smit AB, Verhaagen J (2011) A gene network perspective on axonal regeneration. *Front Mol Neurosci* 4:46.
- van Vliet AC, Lee J, van der Poel M, Mason MRJ, Noordermeer JN, Fradkin LG, Tannemaat MR, Malessy MJA, Verhaagen J, De Winter F (2021) Coordinated changes in the expression of Wnt pathway genes following human and rat peripheral nerve injury. *PLoS One* 16:e0249748.
- Verma P, Chierzi S, Codd AM, Campbell DS, Meyer RL, Holt CE, Fawcett JW (2005) Axonal protein synthesis and degradation are necessary for efficient growth cone regeneration. *J Neurosci* 25:331–342.
- Vogelezang MG, Liu Z, Relvas JB, Raivich G, Scherer SS, Ffrench-Constant C (2001) Alpha4 integrin is expressed during peripheral nerve regeneration and enhances neurite outgrowth. *J Neurosci* 21:6732–6744.
- Vogl AM, Phu L, Becerra R, Giusti SA, Verschuere E, Hinkle TB, Bordenave MD, Adrian M, Heidersbach A, Yankilevich P, Stefani FD, Wurst W, Hoogenraad CC, Kirkpatrick DS, Refojo D, Sheng M (2020) Global site-specific neddylation profiling reveals that NEDDylated cofilin regulates actin dynamics. *Nat Struct Mol Biol* 27:210–220.
- Wei X, Wang X, Zhan J, Chen Y, Fang W, Zhang L, Zhang H (2017) Smurf1 inhibits integrin activation by controlling Kindlin-2 ubiquitination and degradation. *J Cell Biol* 216:1455–1471.
- Werner A, Willem M, Jones LL, Kreutzberg GW, Mayer U, Raivich G (2000a) Impaired axonal regeneration in α7 integrin-deficient mice. *J Neurosci* 20:1822–1830.
- Werner A, Willem M, Jones LL, Kreutzberg GW, Mayer U, Raivich G (2000b) Impaired axonal regeneration in alpha7 integrin-deficient mice. *J Neurosci* 20:1822–1830.
- Winckler B, Faundez V, Maday S, Cai Q, Guimas Almeida C, Zhang H (2018) The Endolysosomal system and proteostasis: from development to degeneration. *J Neurosci* 38:9364–9374.
- Yang WL, Wang J, Chan CH, Lee SW, Campos AD, Lamothe B, Hur L, Grabner BC, Lin X, Darnay BG, Lin HK (2009) The E3 ligase TRAF6 regulates Akt ubiquitination and activation. *Science* 325:1134–1138.
- Zinngrebe J, Montinaro A, Peltzer N, Walczak H (2014) Ubiquitin in the immune system. *EMBO Rep* 15:28–45.